STUDY OF UNSUSPECTED GAMMA RAY ENERGY PEAKS OBSERVED DURING THE DETERMINATION OF THE HALF-LIFE OF ACTIVATED ALUMINIUM

by André P Nel

Submitted to the Department of Electrical Engineering
in partial fulfilment of the requirements for the
Masters Degree in Engineering
Postgraduate Programme in Nuclear Power
University of Cape Town

November 2018

15 January 2019: final version for submission including corrections after examination.

ABSTRACT

In the experimental determination of the half-life of the decay of a radioactive element, an aluminium cylinder is activated through immersion in a thermal neutron bath. The decay of the irradiated aluminium cylinder is then measured to determine the half-life of the resultant ^{28}Al.

During the execution of the experiment, unsuspected gamma ray peaks other than the expected 1.78 MeV from the decay of the activated ^{28}Al are however observed.

Two potential hypotheses are considered in the study. The first hypothesis is that the ^{27}Al from which the aluminium cylinder is manufactured is not pure and contains certain impurities which could be activated resulting in the measurement of the decay of materials other than the intended ^{28}Al. The second hypothesis is the inadequate moderation of the neutrons resulting in the interaction of fast neutrons with the aluminium cylinder and hence the creation of something other than the intended ^{28}Al.

Based on the results of the two experiments conducted, it has been demonstrated that there is some evidence, though not very convincing, that both postulated hypotheses potentially hold true.

Considering the relatively small amounts of alloying elements in a typical aluminium sample and the poor correlation between published half-lives with the derived half-lives from the experiment, the hypothesis that the impurities in the aluminium from which the aluminium cylinder is manufactured are activated when immersed in the neutron bath resulting in the measurement of the decay of materials other than the intended ^{28}Al, is considered possible but improbable.

On the other hand, considering the pertinence of the decay signature of ^{27}Mg in both experiments, the observed increase in the ^{27}Mg activity in the unmoderated activation, the abundance of the target nuclei of ^{27}Al, as well as the increase in the ^{27}Al (n,p) ^{27}Mg reaction with increased neutron energy, hypotheses 2 is deemed both possible and probable.

ACKNOWLEDGEMENT

I would first like to thank my dissertation supervisor Emeritus Professor of Physics, David Aschman from the Physics Department at the University of Cape Town, for his guidance and support during the planning and execution of the experiments as well as the development and review of this mini-dissertation, steering me in the right direction when needed yet allowing this paper to be my own work.

I would also like to thank Dr. John Fearon and Mr Roger Hansen from the Physics Department at the University of Cape Town for the logistical support with the detector setup and cooling without which the experiments could not have been successfully conducted.

I would also like to express my sincere gratitude to Eskom as my employer for the financial support and permission to participate in the Postgraduate Programme in Nuclear Power.

Finally, I would like to express my gratitude to my family and friends for providing me with unfailing support and continuous encouragement throughout my years of study and through the process of researching and writing this dissertation. This accomplishment would not have been possible without them.

Thank You

André P Nel

Table of Contents

List of Tables

List of Figures

PLAGIARISM

I know the meaning of plagiarism and declare that all the work in this document, save for that which is properly acknowledged, is my own. This thesis/dissertation has been submitted to the Turnitin module (or equivalent similarity and originality checker software) and I confirm that my supervisor has seen my report and any concerns revealed by such have been resolved with my supervisor.

Signed by candidate

Chapter 1
Introduction

1.1 Aim

In the experimental determination of the half-life of the decay of a radioactive element, an aluminium cylinder is activated through immersion in a thermal neutron bath. Gamma rays emitted from the decay of the irradiated aluminium cylinder are then measured to determine the half-life of the resultant radioactive isotope ^{28}Al.

The isotope ^{28}Al may be produced by irradiating ^{27}Al, the stable isotope of aluminium, with thermal neutrons, allowing the neutron capture reaction

$$^{27}\text{Al} + n = {}^{28}\text{Al}$$

to occur. The neutron rich isotope ^{28}Al is radioactive and decays to ^{28}Si via beta decay followed by the emission of a 1.78 MeV gamma ray.

During the execution of the experiment, additional gamma-energy signatures other than the expected 1.78 MeV from the decay of the activated ^{28}Al are however observed.

The aim of the project is to determine the reason(s) for the additional gamma energy signatures observed.

1.2 Hypotheses

Two potential hypotheses are considered in an attempt to explain the additional energy readings observed.

The first hypothesis is that the ^{27}Al from which the aluminium cylinder is manufactured is not pure and contains certain impurities. These impurities could also be activated when immersed in the neutron bath resulting in the measurement of the decay of materials other than the intended ^{28}Al.

The second hypothesis is the inadequate moderation of the neutrons by the immersion of the Amercium-Beryllium (AmBe) neutron source in water resulting in the interaction of fast neutrons with the aluminium cylinder and hence the creation of something other than the intended ^{28}Al.

1.3 Hypothesis Testing

The hypothesis dealing with potential impurities in the aluminium will be tested by assuming adequate moderation of the neutrons from the AmBe source. Through neutron activation analysis, the formation of nuclides other than ^{28}Al will be investigated.

The hypothesis dealing with the potential inadequate moderation of the neutrons from the AmBe source will be tested through the analysis of an aluminium cylinder subjected to an AmBe source without any moderation, assuming that the cylinder is manufactured from pure aluminium.

1.4 Overview

The hypothesis dealing with potential impurities in the aluminium is unpacked by providing a brief discussion of:

- The principles of neutron activation analysis, neutron sources and other relevant theory in Chapter 2;
- Overview of aluminium in Chapter 3;
- Description of the experiment in Chapter 4;

- The experimental results are presented in Chapter 5.1 and discussed in Chapter 6.1;
- The final conclusions are drawn in Chapter 7.

The hypothesis dealing with the inadequate moderation of the neutrons draws its background and theory from the sections cited for hypothesis 1 with additional discussions on:

- Moderation of neutrons in section 2.9;
- Fast neutrons in section 2.10;
- Description of the experiment in Chapter 4;
- The experimental results are presented in Chapter 5.2 and discussed in Chapter 6.2;
- The final conclusions are drawn in Chapter 7.

Chapter 2
Theoretical Overview

In this chapter, the theory on a number of topics is explored and summarised which theories forms the basis of the hypotheses developed, the experiments conducted, results analysed and the conclusions drawn.

2.1 Neutron Activation Analysis

Neutron activation analysis was first developed by G. Hevesy and H. Levi in 1936 following the discovery of the neutron by J. Chadwick in 1932. They discovered that the element Dysprosium became radioactive after exposure to a neutron source. They demonstrated that unknown samples can be identified through the measurement of the nuclear reaction decay of the induced radioactivity (Hamidatou *et al.*, 2013).

Neutron activation analysis (NAA) is based on the nuclear physics principles that the nucleus of an atom is stable only when it contains a certain number of neutrons and protons (Keisach, 1972). The number of protons in an atom's nucleus determines an element's identity whereas the number of neutrons usually determines whether the atom is radioactive. Neutron activation analysis is made possible due to the fact that nuclei can absorb additional neutrons, which in many cases, results in the conversion of a stable nucleus to a radioactive nucleus. The excited nucleus de-excites through various decay mechanisms by emitting gamma rays or particles such as alpha or beta particles. Through the detection and analysis of the resultant radioactive decay, the element can be identified (Hamidatou *et al.*, 2013).

This section describes in the first part the basic essentials of neutron activation analysis such as the principles of the NAA method with reference to neutron induced reactions, neutron capture cross-sections, production and decay of radioactive isotopes, nuclear decay and the detection of radiation. In a later part the equipment requirements, gamma-ray detectors, multi-channel analysers and neutron sources are described.

2.2 Neutron Sources

According to (Murray and Holbert, 2015) a common source of neutrons used for calibration and testing purposes is an alpha-neutron material. The alpha-neutron material, named for the alpha-neutron nuclear reaction that occurs within, contains a long-lived alpha-emitter and a lighter target element. Neutrons and gamma rays are released when the alpha particle from the emitter is absorbed by the target.

Examples of alpha-neutron materials are Americium-Beryllium (AmBe) and Plutonium-Carbon (PuC) and also Polonium-Beryllium (used in the initiator of the first nuclear weapon) where the emitter is a high-Z radionuclide and the target is a lighter element. The emitter and target material are either chemically mixed or placed adjacent to one another which enables alpha particles from the emitter to bombard the target. When the bombarding alpha particle has sufficient kinetic energy to overcome the Coulomb barrier of the target, it is absorbed by the target. This absorption of the alpha particle transmutates the target into a different nuclide which is usually in an excited state. One of the primary decay modes of the transmutated target is neutron emission. The decay by neutron emission is usually accompanied by gamma emission as well (Murray and Holbert, 2015).

Because of its relatively high neutron yield, Beryllium is the most common low Z material used in alpha-neutron sources.

The AmBe source is doubly encapsulated. The inner and outer capsules are usually fabricated from stainless steel and the end caps are TIG welded. Space is left within

the inner capsule to allow for the gradual build-up of helium that results from the alpha emissions.

An AmBe radioisotopic source produces neutrons over an energy range from a few eV up to about 11 MeV through the following decay:

$$^{241}Am \rightarrow {}^{237}Np + \alpha$$

The α (^{4}He) from the ^{241}Am decay interacts with the ^{9}Be to produce the neutrons:

$$^{9}Be + {}^{4}He \rightarrow {}^{12}C + n$$

The $^{9}Be + {}^{4}He$ results in the excited compound nucleus $^{13}C^{*}$. This $^{13}C^{*}$ de-excites through 4 main processes, two of which are experimentally unimportant (Odeblad and Nati, 1955). The remaining two processes are indicated below;

$$^{13}C^{*} \rightarrow {}^{12}C + n + 5.6\ MeV$$

$$^{13}C^{*} \rightarrow {}^{12}C + n + \gamma\ (4.4MeV) + 1.2\ MeV$$

The energies can range up to 11 MeV with an average energy between 4 and 5 MeV with prominent 4.4 MeV gamma ray observed during AmBe experiments.

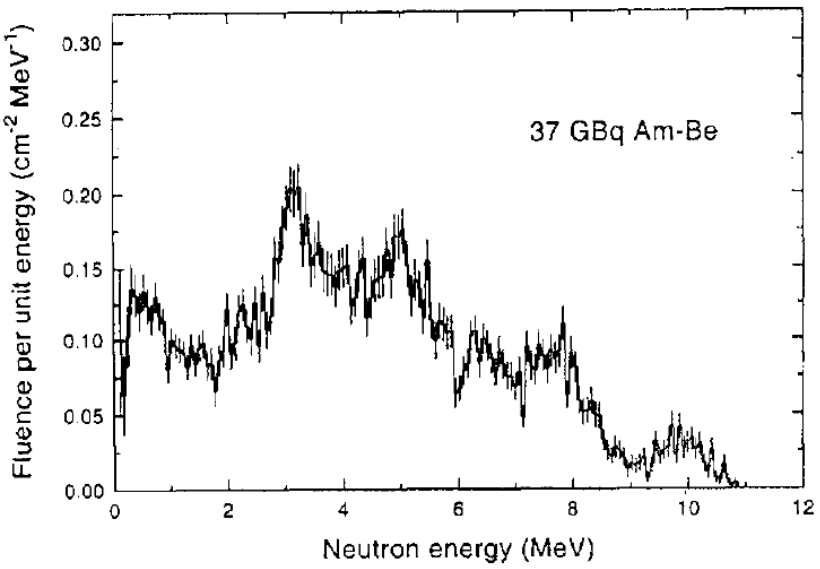

Figure 1 – Measured neutron energy spectrum from a 37GBq AmBe neutron source taken from (Marsh, Thomas and Burke, 1995)

2.3 Neutron Capture

From Nuclear Theory as set out in NucEng CANDU tech docs (Dawson, Fleck and Wadham, 1993), thermal neutrons may be captured by nuclei in an irradiated material. Because the addition of a neutron to a nucleus will change the atomic mass number of the nucleus, the addition of a neutron to a nucleus produces an isotope of that nucleus. The newly formed isotope may be stable like the original nucleus or it may be radioactive, decaying over time to a stable nucleus which may be a different element. For example, Cobalt 59 becomes radioactive Cobalt 60 when it captures a neutron. However, neutron capture by aluminium produces a radioactive isotope which decays to a stable isotope of silicon. Most neutron captures by iron atoms result in a heavier stable isotope of iron.

Thermal neutrons do little structural damage to the crystal lattice of a metal when compared to fast neutrons. Thermal neutrons usually only result in displacement of the nucleus which captured the neutron. After capturing the thermal neutron, the nucleus is in an excited or high energy state. The excess energy is released by emitting gamma rays with the result that the emitting nucleus recoils and is displaced within the crystal lattice.

2.4 Neutron Capture Cross Section

As described in (Lewis, 2008) neutrons are electrically neutral particles. The neutron's flight is therefore not affected by either the electrons surrounding a nucleus nor the electric field generated by a positively charged nucleus. Neutrons will therefor travel in straight lines and only deviate from their path when they actually collide with a nucleus. This collision will scatter the neutron into a new direction or the neutron can be absorbed into the nucleus. An ejected neutron will typically undergo a number of scattering collisions followed by absorption at which time its identity is lost. Since the nucleus of an atom has a radius of only in the order of 10^{-12}cm when compared to the radius of typically 10^{-8}cm of an atom, the fraction of the

cross-sectional area perpendicular to a neutron's flight path blocked by a single tightly packed layer of atoms would be roughly 10^{-8}. Even when traveling through a solid material, the material thus appears to be quite empty to a neutron's flight. On average neutrons therefor penetrate many millions of layers of atoms between collisions with nuclei.

The distance that a neutron travels before it collides and/or is absorbed has a probabilistic interpretation. As the probability of a neutron colliding within a certain distance is independent of its past history, the mean free path (denoted by λ), i.e. the mean distance travelled by a neutron between collisions, can be calculated. The total macroscopic cross-section is inversely proportional to the mean fee path (Lewis, 2008).

From (IAEA-TECDOC-1340, 2003) the neutron interaction with the nucleus of the target material can be expressed quantitatively in terms of the nuclear cross-section. This cross-section is a measure of the probability that the given reaction (e.g. scattering, absorption, etc) will take place. This cross-section can be expressed in terms of an imaginary cross-sectional area perpendicular to a beam of neutrons which is presented by the nucleus. The nuclear reaction will only take place if the neutron passes through this imaginary cross-sectional area. The unit of the cross-section is barn where 1 barn = $10^{-24}cm^2$.

The cross-sectional area is dependent on the energy of the neutrons and varies from nucleus to nucleus. In general, the slower the speed of the neutron, the greater the probability for a reaction to occur. Neutrons that have lost energy, primarily through elastic scattering, to thermal energy ranges, have the maximum value for the cross-section. In this thermal energy region, the cross-section varies as $\frac{1}{v}$, where v is velocity of neutrons.

The cross-section values are quoted at room temperature (20°C). The temperature dependence of the cross-section is corrected through the following relationship:

$$\sigma = \sigma_0 \left(\frac{T_0}{T} \right)^{\frac{1}{2}}$$

Where σ is the cross-section at temperature T and σ_0 the cross section at temperature T_0. The temperature can therefore have a significant impact on the cross-section.

2.5 Production and decay of radioactive isotopes

The n-γ reaction is the fundamental reaction for neutron activation analysis. Consider the following reaction:

$$^{58}Fe + {}^{1}n \rightarrow {}^{59}Fe^{*} \rightarrow {}^{59}Co + \beta^{-} + \gamma$$

In the above example, ^{58}Fe is a stable isotope of iron whilst ^{59}Fe is a radioactive isotope of iron. The gamma rays that are emitted during the decay of the ^{59}Fe nucleus are characteristic for this nuclide and have energies of 142.4, 1099.2, and 1291.6 keV.

As mentioned in section 2.4, the probability of a neutron interacting with a nucleus is a function of the neutron energy. The probability for a neutron being captured is referred to as the capture cross-section, and each nuclide has its own neutron energy-capture cross-section relationship. The capture cross-section is generally the greatest for low energy neutrons, referred to as thermal neutrons as they are in thermodynamic equilibrium with their surroundings. At room temperature, the thermal neutron mean energy is approximately 0.025 eV with speeds in the region of 2.2×10^{3} m s^{-1}. Under the above mentioned conditions, further scattering of the neutrons does not change their average kinetic energy which is equal to (3/2)kT,

where k is the Boltzmann constant (1.3806×10^{-23} J K^{-1}) and T is the absolute temperature in Kelvin (*Nuclear Physics - Department of Physics - University of Liverpool*, no date).

Although some nuclides have greater capture cross-sections for higher energy neutrons (epithermal neutrons), routine neutron activation analysis is generally applied to nuclides that are activated by thermal neutrons.

2.6 Nuclear decay and the detection of radiation

According to Canada's national laboratory for particle and nuclear physics and accelerator-based science (TRIUMF, no date), there are a number of modes under which a radioactive nucleus can decay, the most prominent which are quoted below from (TRIUMF, no date):

β^+ decay

$${}^{A}_{Z}\mathrm{X} \rightarrow {}^{A}_{Z-1}\mathrm{X}^{*} + \mathrm{e}^{+} + \nu_{\mathrm{e}}$$

The weak interaction causes a proton in a nucleus to spontaneously turn into a neutron, a positron and an electron neutrino. The nucleus is often left in an excited state and loses energy by emitting gamma rays. β^+ decay occurs in nuclei on the neutron-deficient side of the nuclear chart (*Live chart - Table of Nuclides - Nuclear structure and decay data*, 2018).

β^- decay

$${}^{A}_{Z}\mathrm{X} \rightarrow {}^{A}_{Z+1}\mathrm{X}^{*} + \mathrm{e}^{-} + \bar{\nu}_{\mathrm{e}}$$

A neutron spontaneously turns into a proton, an electron and an anti-electron neutrino. The daughter nucleus is often formed in an excited state and loses energy

by gamma-ray emission. β^- decay occurs in nuclei on the neutron-rich side of the nuclear chart, that is nuclei containing an excess of neutrons compared to protons.

Electron Capture

$${}^{A}_{Z}\mathrm{X} + \mathrm{e}^- \rightarrow {}^{A}_{Z-1}\mathrm{Y}^* + \nu_\mathrm{e}$$

A proton in a nucleus spontaneously and simultaneously captures an atomic electron and turns into a neutron and emits an electron neutrino. The daughter nucleus is often formed in an excited state and loses energy by gamma-ray emission. Electron capture competes with β^+ decay on the neutron-deficient side of the nuclear chart, that is nuclei with an excess of protons to neutrons.

Double β^- Decay

$${}^{A}_{Z}\mathrm{X} \rightarrow {}^{A}_{Z-2}\mathrm{Y} + 2\mathrm{e}^- + 2\bar{\nu}_\mathrm{e}$$

Two neutrons in a nucleus spontaneously and simultaneously turn into two protons, two electrons and two electron-type anti-neutrinos. The daughter nucleus is often formed in an excited state and loses energy by gamma-ray emission. Double β^- decay is an extremely rare process and occurs in nuclei which appear to be stable to other decay modes.

α Decay

$${}^{A}_{Z}\mathrm{X} \rightarrow {}^{A-4}_{Z-2}\mathrm{Y} + {}^{4}_{2}\mathrm{He}$$

A nucleus spontaneously emits a ^{4}He nucleus - a tightly bound system of two protons and two neutrons. The daughter nucleus is often formed in an excited state and loses energy by gamma-ray emission or Internal conversion process (see later). Alpha decay usually occurs in heavy nuclei.

γ Ray Emission

$${}^{A}_{Z}\mathrm{X}^{*} \rightarrow {}^{A}_{Z}\mathrm{X} + \gamma$$

A nucleus in an excited state loses energy by emitting a gamma ray. A gamma ray is a high energy photon which is essentially a packet of energy. Gamma-ray emission can occur in any nucleus on the nuclear chart. An alternative process in certain transitions is internal conversion.

Internal Conversion

A nucleus in an excited state loses energy by passing it to an atomic electron and ejecting it from the atom. The energy of the electron is equal to the transition energy minus the binding energy of the atomic orbital from which it came. Internal conversion can occur in any nucleus on the nuclear chart but is more common in heavy nuclei above Lead. An alternative process for the nucleus to lose energy is gamma ray emission.

The common denominator in all the above-mentioned mechanisms of decay is the emission of gamma rays during the de-excitation process.

2.7 Gamma Radiation

As described in (Reilly, Ensslin and Smith, 1991), gamma rays are high-energy electromagnetic radiation emitted in the de-excitation of the atomic nucleus. It can be described as a wave phenomenon involving electric and magnetic field oscillations. Gamma rays have typical frequencies of 10^{18} Hz and energy of 10 keV and above.

Gamma rays from nuclear decay are emitted with a rate and energy spectrum unique to the nuclear isotope that is decaying. This uniqueness provides the basis for most gamma ray assay techniques.

In gamma decay, depicted in Figure 2 below, a nucleus changes from a higher energy state to a lower energy state through the emission of electromagnetic radiation (photons). The number of protons (and neutrons) in the nucleus does not change in this process, so the parent and daughter atoms are the same chemical element. In the gamma decay of a nucleus, the emitted photon and recoiling nucleus each have a well-defined energy after the decay. The characteristic energy is divided between only two particles (Murray and Holbert, 2015).

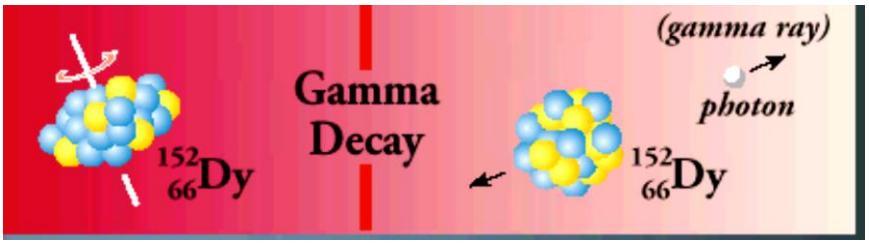

Figure 2 – Gamma Decay taken from (Murray and Holbert, 2015)

As described in (Reilly, Ensslin and Smith, 1991), the number of unstable nuclei decays exponentially with time and is represented by the following relationship:

$$n = n_0 e^{-\lambda t} \quad (2.1)$$

where:

n = the number of nuclei at time t

n_0 = the number of nuclei at t=0

λ = the decay constant.

The time required for the number of nuclei to decay to half its original number is known as the half-life and is related to the decay constant as indicated below:

$$T_{½} = (\ln 2) / \lambda \quad (2.2)$$

Equations 2.1 and 2.2 form the basis of Instrumental Neutron Activation Analysis.

2.8 Measurement of Radioactive Decay

Unlike visible light, gamma rays cannot be detected directly. A medium has to be setup that interacts with the gamma ray and another to detect the effects from the interaction.

From (Martin, 2006) solid-state detectors operate through the promotion of electrons from the valence band of a solid to the conduction band as a result of the entry of the incident particle into the solid. The resulting absence of an electron in the valence band (commonly referred to as a 'hole') behaves like a positron. Semiconductor detectors are essentially solid-state ionization chambers with the electron–hole pairs playing the role of electron–ion pairs in gas detectors. In the presence of an electric field, the electrons and holes separate and collect at the electrodes, giving a signal proportional to the energy loss of the incident charged particle. Most semiconductor detectors use the principle of the junction diode having a P-I-N structure in which the Intrinsic (I) region is sensitive to ionizing radiation, particularly X-rays and gamma rays. Under reverse bias, an electric field extends across the intrinsic or depleted region. When photons interact with the material within the depleted volume of a detector, charge carriers (holes and electrons) are produced and are swept by the electric field to the P and N electrodes. This charge, which is in proportion to the energy deposited in the detector by the incoming photon, is converted into a voltage pulse by an integral charge sensitive preamplifier (Reguigui, 2006).

Since the band gap in some solids is as small as 1 eV and the energy loss required to produce a pair is only 3–4 eV on average (cf. the 30 eV required in a gas detector), a very large number of electron–hole pairs with only a small statistical fluctuation will be produced by a low-energy particle. Solid-state detectors are therefore very useful in detecting low-energy particles. Semiconductors (principally silicon or germanium) are used as a compromise between materials that have residual conductivity sufficient to enable conduction pulses due to single particles to be distinguished above background and those in which the charge carriers are not rapidly trapped in impurities in the material.

The major drawback of germanium detectors is that they must be cooled to liquid nitrogen temperatures to produce spectroscopic data. At higher temperatures, the

electrons can easily cross the band gap in the crystal and reach the conduction band, where they are free to respond to the electric field, producing too much electrical noise to be useful as a spectrometer. Cooling to liquid nitrogen temperature (77 K) reduces thermal excitations of valence electrons so that only a gamma ray interaction can give an electron the energy necessary to cross the band gap and reach the conduction band. This cooling of the detector is achieved by mounting the detector on a “cold finger” which is immersed in liquid nitrogen.

The complete detector and preamplifier assembly mounted on its cold finger can then be fixed onto a suitable liquid nitrogen reservoir by an arrangement, such as that shown in Figure 3.

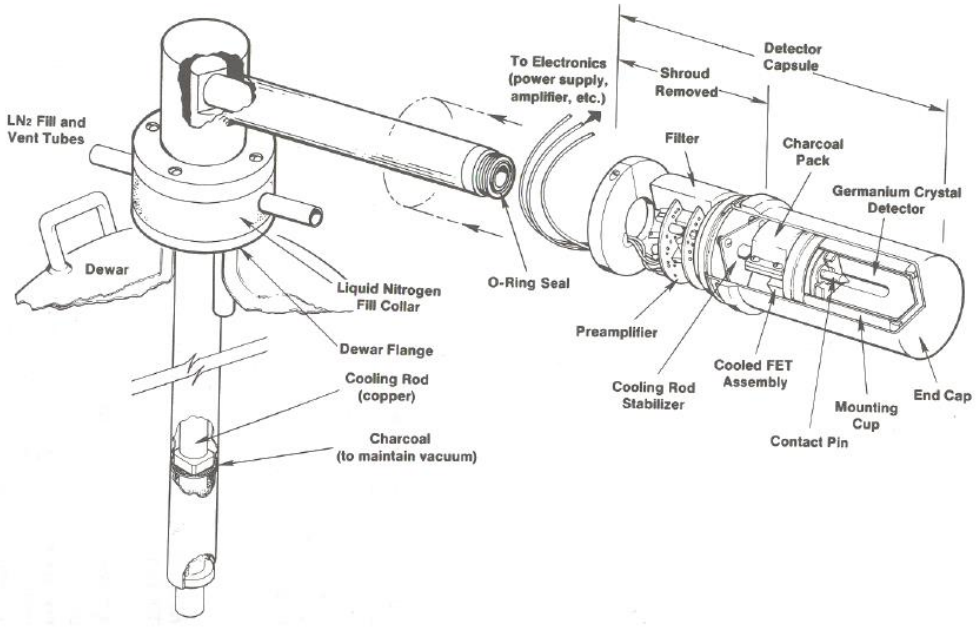

Figure 3 - Arrangement of detector and preamplifier within the cryostat housing as illustrated in (Gilmore, 2008)

2.9 Neutron moderation

From (Bodansky, 2004), neutron moderation or thermalisation is described as the reduction of the energy level of neutrons to thermal energy ranges, primarily through elastic scattering of the neutron within the moderator.

The energy transfer in an elastic nuclear collision depends on the angle at which the incident neutron is scattered. The energy of the scattered neutron can be calculated based on the principles of the conservation of energy and momentum based on the kinematics of “billiard ball” collisions. Based on the above-mentioned principles, if a neutron of initial energy is scattered at 0° by a nucleus of the moderator material, namely it continues in the forward direction, then the energy of the scattered neutron will remain the same. The maximum energy loss is achieved if the neutron is scattered at 180°.

In (Bodansky, 2004) it is shown that the ratio of the average scattered neutron energy to initial neutron energy is represented by δ which is:

$$\delta = (A^2 + 1) / (A^2 + 2A + 1) \qquad (2.3)$$

To minimize the loss of neutrons by absorption, it is desirable that the thermalization of the neutrons be accomplished in as few collisions as possible. An effective moderator that reduces the neutron energy with relatively few collisions requires a low value of the parameter δ. Based on the relationship given above, this means that the moderator must have a relatively low atomic mass number A.

Hydrogen, in the form of ordinary or “light” water, is thus an obvious choice for use as a moderator in light of the above relationship. The oxygen in the water is relatively inert, having a very low capture cross section and being much less effective than hydrogen as a moderator.

Ordinary hydrogen has however a major drawback of having a large cross section (0.33 b at 0.0253 eV) for the capture reaction:

$$n + {}^{1}H \rightarrow {}^{2}H + \gamma \qquad (2.4)$$

With the moderating ratio for light water being 71, coupled with its cheap availability, is the reason for the use of light water as the moderator in the experimental testing of hypothesis 1.

2.10 Fast Neutrons

From (Gilmore, 2008), certain neutron-induced reactions will involve energetic or fast neutrons, where the extra kinetic energy is needed to knock out additional particles from the atom.

Common fast neutron reactions are (n, p), (n, α) and (n, 2n). Figure 4 shows these transformations on the Z against N nuclide chart format.

The quantity of radioactivity formed by these reactions is often small because of relatively low fluxes of fast neutrons and small cross-sections. However, reactor operators and persons involved in reactor decommissioning will be aware of the significant amounts of activity that can be formed by certain reactions, such as:

^{54}Fe (n, p) ^{54}Mn,

^{58}Ni (n, p) ^{58}Co and

^{27}Al (n, α) ^{24}Na.

The likelihood of the production of all these radionuclides can again be followed on the nuclide chart.

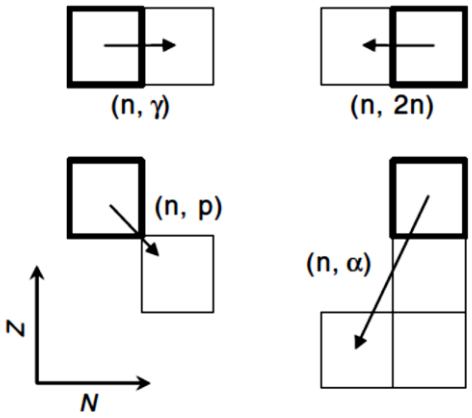

Figure 4 - Location of products of neutron reactions. Bold boxes indicate the stable target nuclides (Gilmore, 2008)***.***

2.11 Radioactive decay and Half Life

As described in (Lilley, 2001), the probability that a nucleus will decay in any given time interval is described by the decay constant (λ) which is stated in per unit time. If there are N radioactive nuclei in a sample, the rate of decay is given by the following relationship:

$$dN/dt = -\lambda N \tag{2.5}$$

The negative sign indicating that the number of radioactive nuclei is decreasing with time. The solution to the above equation is:

$$N(t) = N_0 * e^{-\lambda t} \tag{2.6}$$

where

N(t) is the number of nuclei at time t

N0 is the number of nuclei at time t = 0

λ is the decay constant.

As described in (Lewis, 2008), a commonly and more intuitive descriptor is the half-life which is defined as the time is takes for one half of the original amount of nuclei to decay. By substituting $N_{½} = N_0/2$ into the decay equation and by applying the mathematical rules for logarithms yields the following relationship for the half-life of nuclei:

$$t_{½} = \ln(2) / \lambda \tag{2.7}$$

Since the half-life is constant and characteristic for every radionuclide, it is a useful parameter in Neutron Activation Analysis and assists in the identification of the isotopes of interest.

Chapter 3
Aluminium Overview

According to AluMatter (AluMatter, 2013), aluminium is not 100% pure as it contains certain residual impurities, the most common being iron, silicon and copper.

Iron and silicon have low solid solubility in aluminium and form fine segregates at the cellular boundaries during solidification. Depending on their size, distribution and reactivity, such segregates influence the local properties of the oxide film. These give rise to nanoscale texture patterns after alkaline surface cleaning or polishing. The ridges of such texture patterns are preferred sites for nucleation of pits.

Copper in low concentrations is present in solid solution, however at higher concentrations copper also segregates at cell boundaries.

According to United Aluminium, (United Aluminium, 2013) Aluminium alloys are identified by a four-digit numerical system which is administered by the Aluminium Association (The Aluminum Association, 2018). The alloys are conveniently divided into eight groups based on their principal alloying element. The first digit identifies the alloy group as follows:

ALLOY GROUP	PRINCIPAL ALLOYING ELEMENT	Comment
1xxx	Unalloyed Aluminium	Purity of 99.0% or Greater
2xxx	Copper	Heat Treatable Alloys
3xxx	Manganese	
4xxx	Silicon	Low Melting Point Alloys
5xxx	Magnesium	
6xxx	Magnesium and Silicon	Heat Treatable Alloys
7xxx	Zinc	Heat Treatable Alloys
8xxx	Other Elements	

Table 1 – Aluminium Alloy Identification

The last two digits in the 1xxx group correspond with the two digits after the decimal which indicate the minimum aluminium content. For example, the aluminium content of 1060 is 99.60% minimum, 1100 is 99.00% minimum, 1350 is 99.50% minimum and so on.

3.1 Composition of Aluminium

The Aluminium Association based in Washington, DC (The Aluminum Association, 2018) provides amongst others, the limits for natural impurities in aluminium as well as the chemical composition limits for aluminium alloys. Impurity limits are set by the Aluminium Association (The Aluminum Association, 2018) and Global Metals (Global Metals, 2011) for the elements as indicated in the table 3.

	Aluminium Association	Global Metals
Si	√	√
Fe	√	√
Cu	√	√
Mn	√	√
Mg	√	√
Cr	√	√
Ni	√	
Zn	√	√
Ti	√	√
Ag	√	
B	√	
Bi	√	
Ga	√	
Li	√	
Pb	√	
Sn	√	
V	√	
Zr	√	

Table 2 – Impurity limits set by both The Aluminium Association and Global Metals

The analysis of potential impurities will therefore be guided by the typical impurities for which limits are set by both the Aluminium Association and Global Metals these being:

Si, Fe, Cu, Mn, Mg, Cr, Zn and Ti

This does not imply that other impurities are not present or cannot be detected but is used to narrow the field of the investigation for the experiment.

Various standards exist worldwide for the fraction of impurities and other elements for the various aluminium alloys. To establish an expected order of impurities, the

nominal compositions of common wrought aluminium alloys are listed below (Davis, 2001):

Element	Composition limits
Mg	0.5 - 5.1%
Si	0.1 – 5%
Fe	up to 1.1%
Cu	0.1 - 6%
Zn	1 – 7.6%
Cr	0.1 - 0.26%
Ti	up to 0.15%
Mn	0.1 - 1.2%

Table 3 - Nominal compositions of common wrought aluminium alloys

As published by Digital Library for Earth System Education Community Services Centre (Eby, 2017) certain elements are more readily analysable by neutron activation analysis due to, for example, the limitation of short half-lives. A periodic table showing elements that can be analysed by neutron activation analysis is shown in Figure 5 with the typical expected impurities from Table 3 highlighted.

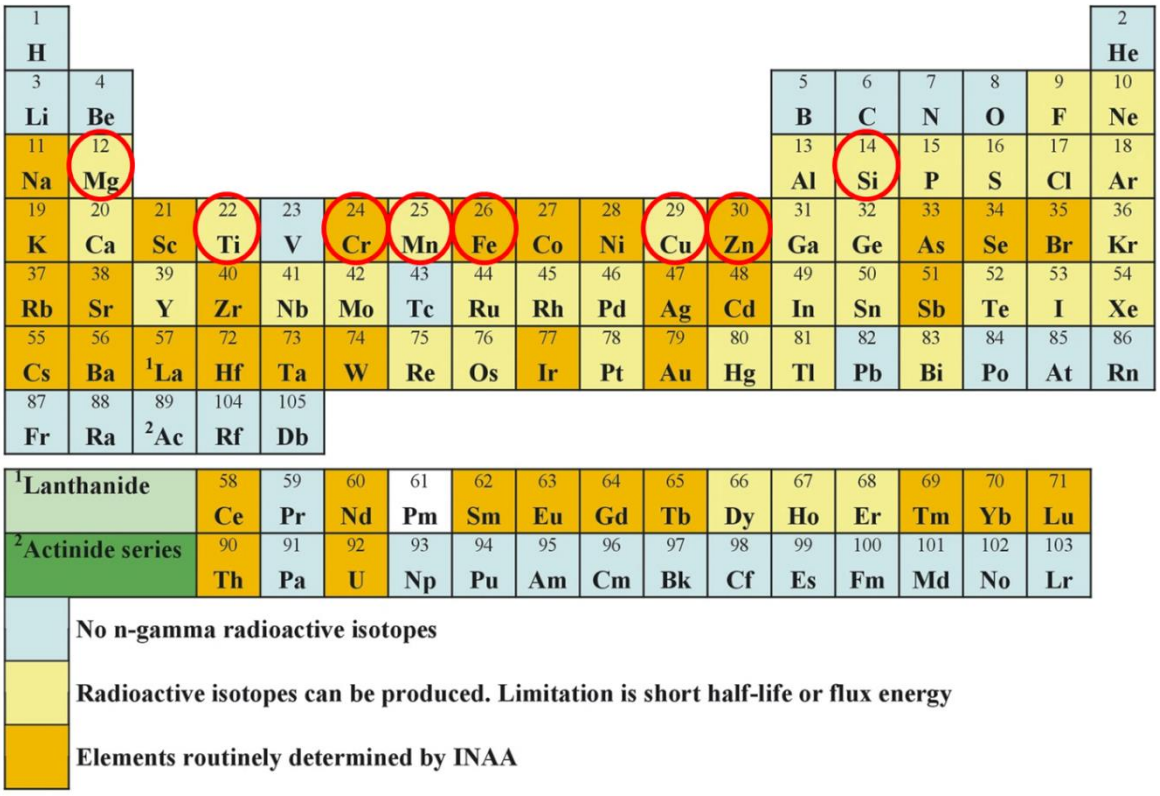

Figure 5 - Elements that may be analysed via INAA taken from (Eby, 2017).

All eight elements selected based on commonality as typical impurities for which limits are set by both the Aluminium Association (The Aluminum Association, 2018) and Global Metals (Global Metals, 2011) are thus suitable for evaluation in INAA.

3.2 Evaluation of Suitable Isotopes for INAA

From the US NRC webpage (USNRC, 2009), the following factors affecting neutron activation need to be considered during the experiment:

a. Stability of the reaction product

b. Half-life of the activation product

c. Radiation emitted by the activation product

d. Cross section of the target nuclide

e. Abundance of the target nuclide

f. Neutron fluence rate (and mass of target element)

The following explanations are quoted from the US NRC webpage (USNRC, 2009) and are used to illustrate the typical factors which informs the assessment set out in section 3.3:

a. Stability of the reaction product

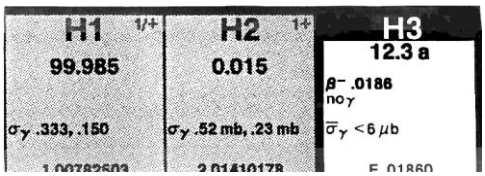

If ^{1}H absorbs a neutron, it simply becomes ^{2}H which is stable.

However, when ^{2}H (deuterium) absorbs a neutron, it becomes ^{3}H (tritium) which is radioactive. This is the reaction of importance. Examples would be the production of tritium at heavy water reactors and tritium in the oil of pumps at accelerators.

b. Half-life of the activation product

If the exposure of the target to neutrons is continuous, the activation product activity increases and eventually reaches a maximum equilibrium activity when the rate of production equals the rate of decay. As an approximation, this equilibrium is achieved after the neutron exposure has continued for five half-lives of the product.

For situations when the exposure is brief, the shorter the half-life of the activation product, the greater its activity at the end of activation. The long half-live of tritium (12.3 years) means that short exposures to neutrons will produce almost no activity.

c. Radiation emitted by the activation product

The radiation emitted by the activation product will affect the hazard associated with its production and the methods by which it can be detected. The beta particles

emitted by tritium are of such a low energy (18.6 keV max) that they cannot be detected by conventional survey instruments. In addition, there is no gamma ray emitted when tritium decays.

d. Cross section of the target nuclide

The cross section of a reaction reflects the probability of the reaction. The latter depends on the energy of the neutrons and the identity of the target nuclide.

e. Abundance of the target nuclide

Towards the top of the box of a stable nuclide, the chart indicates the percent abundance – the percent of the element's mass that consists of the nuclide.

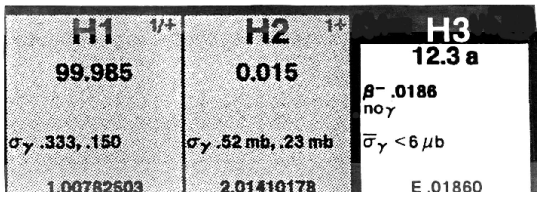

The above shows that only 0.015 percent of natural hydrogen (by mass) is ^{2}H. This means that there is very little ^{2}H in hydrogen that would serve as a target for tritium production.

f. Neutron fluence rate (and mass of target element)

The greater the neutron fluence rate, the greater the induced activity of the activation product. In addition, the greater the mass of the target element (and the number of target atoms), the greater the induced activity of the activation product.

Radiative capture of a neutron in ^{1}H (n,γ) ^{2}H has been used as a particular simplistic example to illustrate the important factors in neutron activation analysis. This mini-dissertation describes the neutron activation of aluminium.

The ^{27} Al (n,γ) reaction is suitable for experimental study in a university laboratory because of the following:

i. Natural aluminium is monoisotopic (^{27}Al), available in easily machined metallic form, and fairly cheap.

ii. An Am-Be source can provide a simple source of both fast and slow neutrons (the latter if a water bath is used for moderation).

iii. The ^{27}Al (n,γ) reaction has a good cross-section for thermal neutron energies.

iv. The daughter nucleus (^{28}Al) has a convenient beta minus decay, with a half-life 134 seconds.

v. The beta minus daughter ^{28}Si*, decays by gamma ray emission

$$^{28}\text{Si}^* \rightarrow {}^{28}\text{Si}^* + \gamma$$

with a gamma ray energy of some 1780 keV which is easily detected with either a scintillation counter such as sodium iodide, or a high-resolution detector such as a high purity germanium solid state detector.

3.3 Assessment Potential of Probable Impurities

In this section, the naturally occurring isotopes of the eight identified elements are assessed for their potential to be activated through thermal neutron absorption and hence the ability to detect the subsequent decay through the measurement of the associated gamma rays.

Both the visual extracts from the Period Table and the decay drawings are taken from the Table of Isotopes (Firestone *et al.*, 1996).

3.3.1. Iron (Fe)

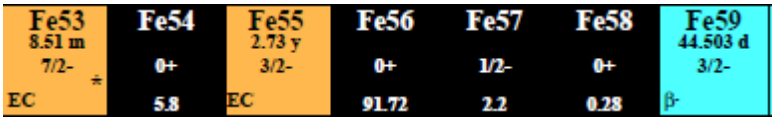

Iron has four naturally occurring isotopes. Beginning with ^{54}Fe serving as the potential target nuclide, neutron irradiation produces ^{55}Fe (the activation product). Although radioactive, ^{55}Fe has a long half-life (2.73 years).

For significant production of ^{55}Fe, very long exposure periods would be required. Even if it could be produced in significant quantities, ^{55}Fe decays exclusively by electron capture (ε) which means that no gamma rays are emitted with which we could detect and identify its presence.

The next stable nuclide of Iron that could be considered as a potential target is ^{56}Fe. Neutron absorption in the ^{56}Fe in the sample is however simply converted to another stable nuclide, ^{57}Fe.

Similarly, any ^{57}Fe present in the sample will be converted into a stable product, ^{58}Fe.

If NAA is going to detect the presence of iron with any degree of sensitivity, it must be done by the conversion of ^{58}Fe into ^{59}Fe.

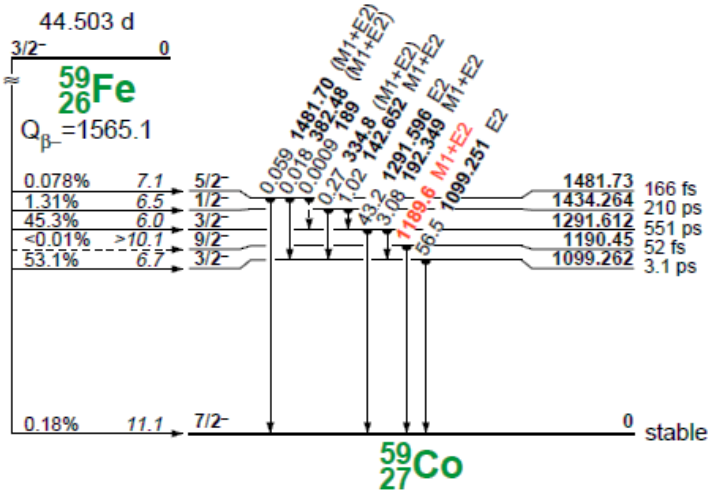

The half-life of ^{59}Fe (44.5 days) is a bit long. ^{59}Fe emits gamma rays at 1099.3 and 1291.6 keV with intensities of 53% and 45% respectively when it β^- decays to ^{59}Co as shown. The cross section of the target, ^{58}Fe, is 1.2 barns.

The problem with ^{58}Fe as target material lies in the low abundance of 0.28% of naturally occurring isotope of iron. As such, the detection of trace quantities of iron requires high neutron fluence rates.

3.3.2. Manganese (Mn)

Manganese has only one stable nuclide, ^{55}Mn, with an abundance of 100%.

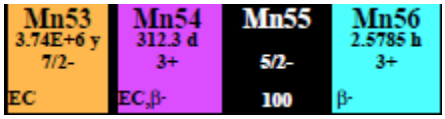

The ^{55}Mn cross section for neutron capture is high being 13.3 barns. ^{56}Mn, the activation product, has a half-life of 2.578 hours and emits a gamma ray of 846.8 keV when β^- decaying to ^{56}Fe.

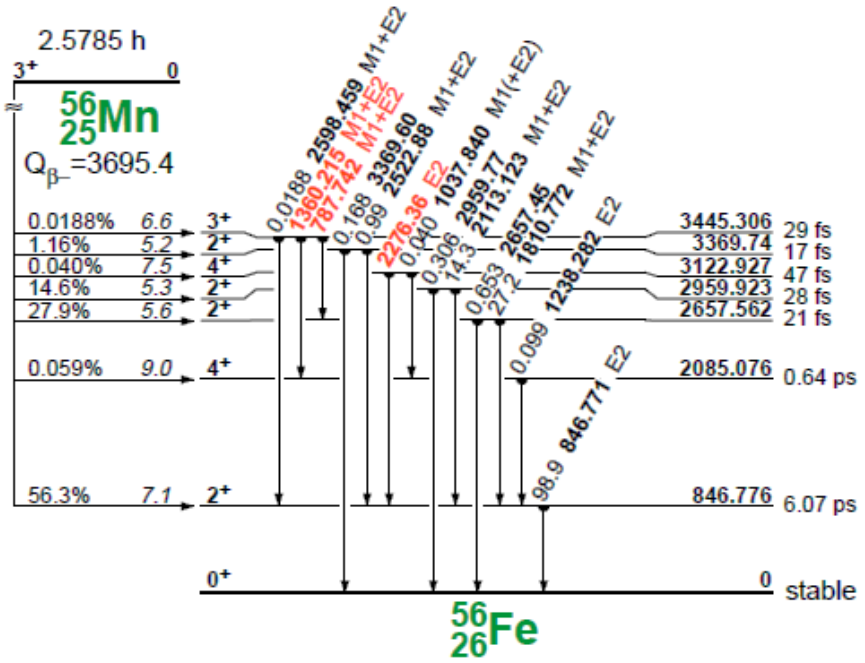

3.3.3. Titanium (Ti)

Titanium has 5 naturally occurring isotopes ^{46}Ti, ^{47}Ti, ^{48}Ti, ^{49}Ti and ^{50}Ti.

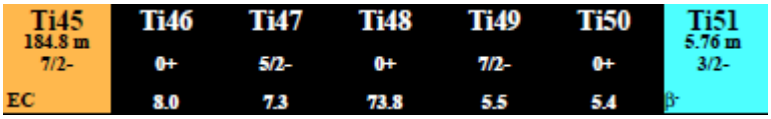

Neutron absorption in 95% of the stable isotopes (percentage naturally occurring) results in the formation of another stable isotope of Titanium. The only naturally occurring isotope of Titanium that can be activated by neutron absorption is ^{50}Ti to form ^{51}Ti which β^- decays to ^{51}V releasing 928.6, 608.6 and 320.1 MeV gamma rays as shown.

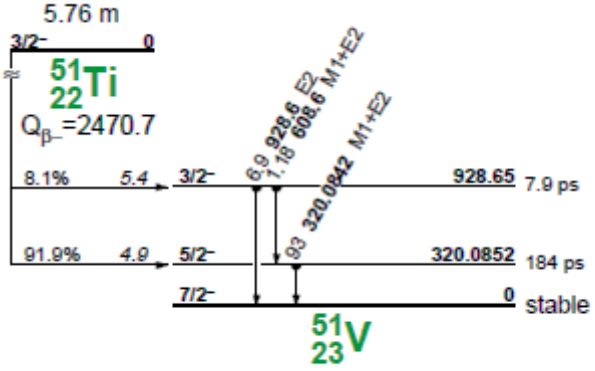

3.3.4. Copper

Natural occurring stable isotopes of Copper are ^{63}Cu and ^{65}Cu.

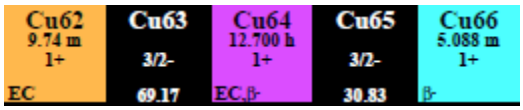

Neutron capture in ^{63}Cu produces the radioactive isotope ^{64}Cu which decays to ^{64}Ni and ^{64}Zn through electron capture and β^+ (61%) and through β^- (39%) decay respectively as indicated below. The decay to ^{64}Ni emits a gamma ray at 1345.8 MeV.

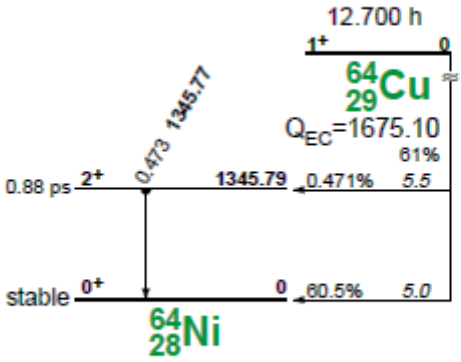

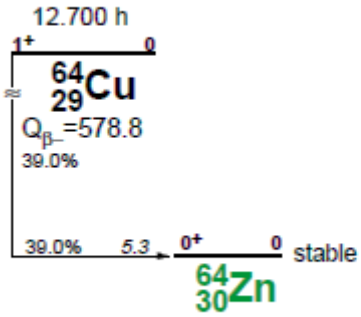

Neutron capture in ^{65}Cu produces the radioactive isotope ^{66}Cu which decays to ^{66}Zn through β^- decay. The decay to ^{66}Zn emits gamma rays at 1039 and 833.5 MeV as indicated below.

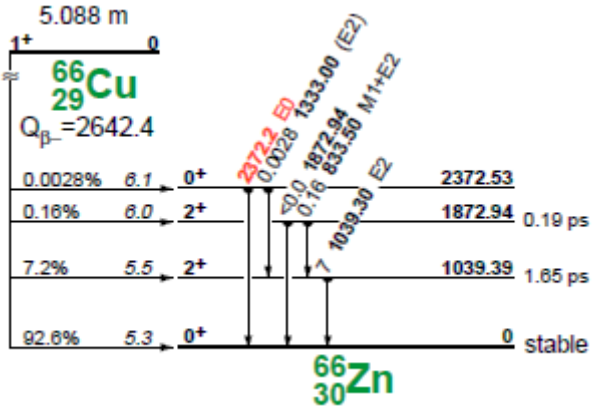

3.3.5. Zinc

Natural occurring stable isotopes of Zinc are ^{64}Zn, ^{66}Zn, ^{67}Zn, ^{68}Zn and ^{70}Zn.

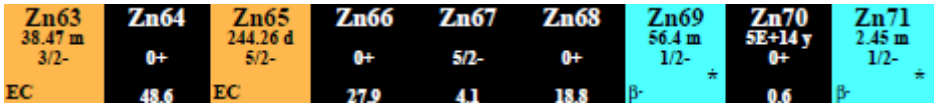

Neutron capture in ^{64}Zn produces the radioactive isotope ^{65}Zn which decays to ^{65}Cu through electron capture and β^+ decay emitting gamma rays at 1115.5 MeV as illustrated below.

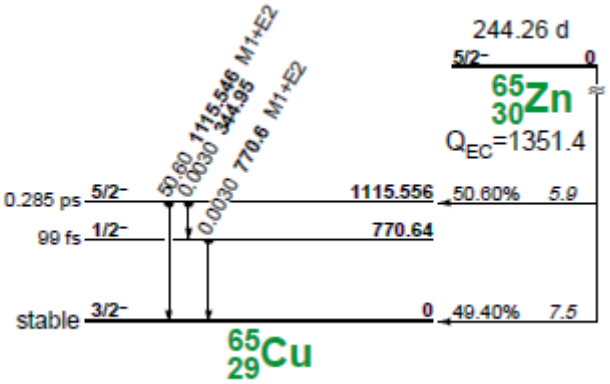

Neutron capture in ^{68}Zn produces the radioactive isotope ^{69}Zn which decays to ^{69}Ga through β^- decay emitting gamma rays at 318.7 and 872.1 MeV as illustrated below.

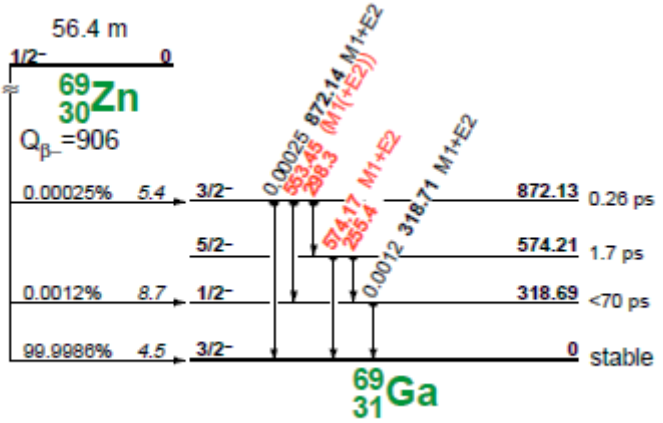

Neutron capture in ^{70}Zn produces the radioactive isotope ^{71}Zn which decays to ^{71}Ga through β^- decay emitting a host of gamma rays. Gamma ray with intensity above 2% listed below:

121.5 (3.0%), 389.8 (3.8%), 511.5 (32%), 910.2 (7.8%), and 1119.6 (2.18%) MeV.

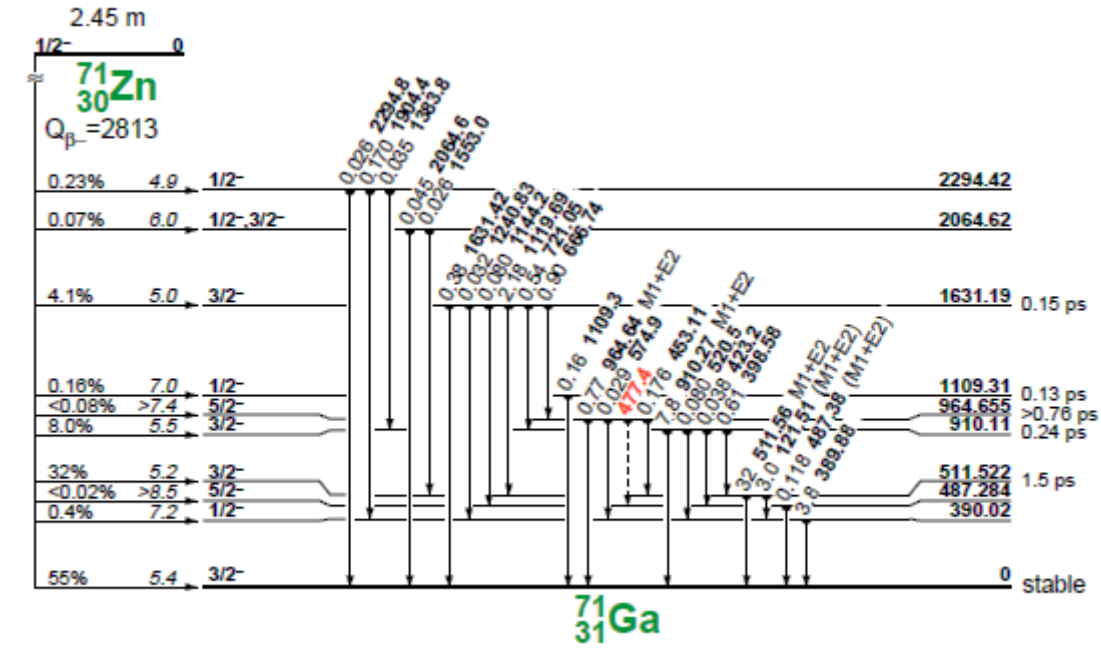

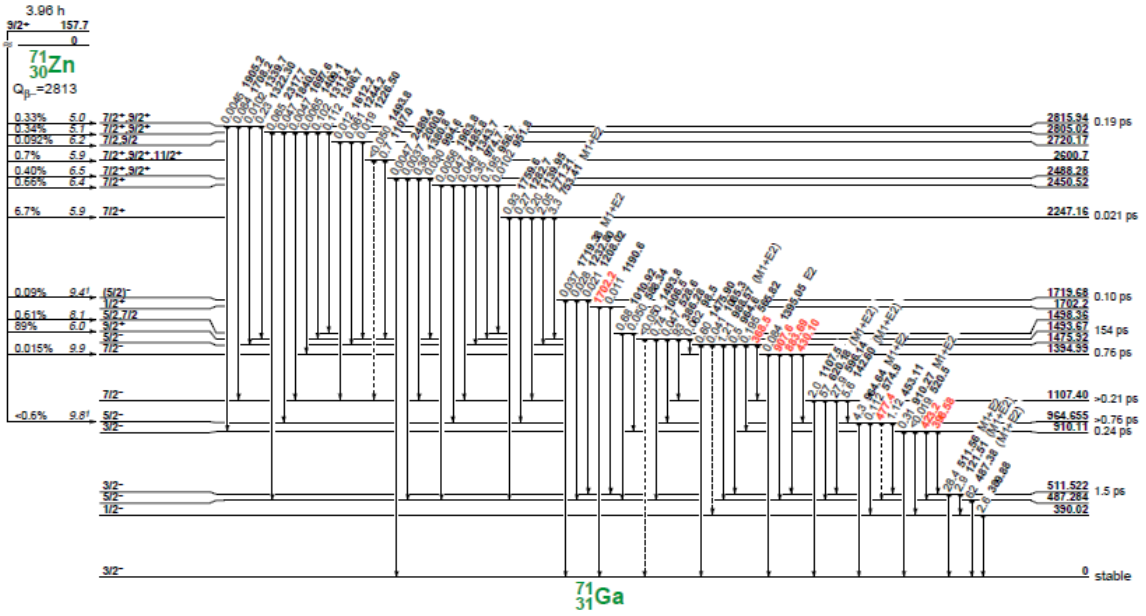

3.3.6. Chromium

Chromium has four naturally occurring isotopes being ^{50}Cr (4.4%), ^{52}Cr (83.8%), ^{53}Cr (9.5%) and ^{54}Cr (2.3%) (^{50}Cr being radioactive with a half-life of 1.8E+17 years).

Cr49	Cr50	Cr51	Cr52	Cr53	Cr54
42.3 m	1.8E+17 y	27.702 d			
5/2-	0+	7/2-	0+	3/2-	0+
	ECEC				
	4.345	EC	83.789	9.501	2.365

Neutron capture in ^{50}Cr produces the radioactive isotope ^{51}Cr which decays to ^{51}V through electron capture emitting a gamma ray at 320 MeV as illustrated below.

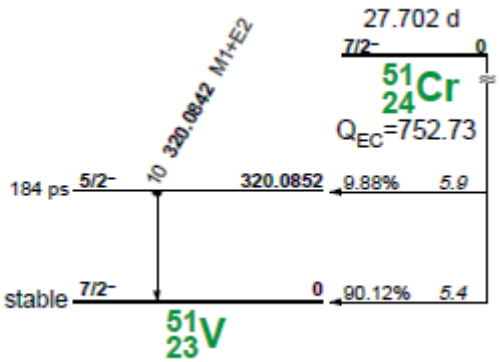

Neutron capture in ^{52}Cr results in the production of the stable isotope ^{53}Cr and neutron capture in ^{53}Cr results in another stable isotope ^{54}Cr.

Neutron capture in ^{54}Cr produces the radioactive isotope ^{55}Cr which decays to ^{55}Mn through β^- decay emitting a host of low intensity gamma rays (none higher than 0.03%).

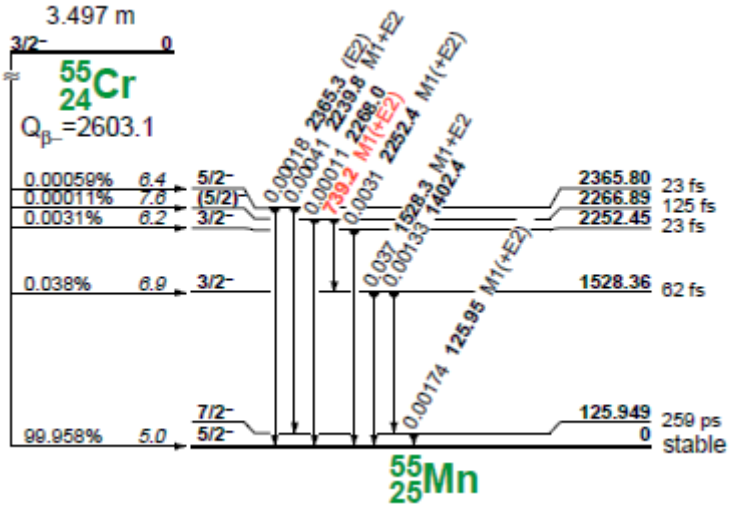

3.3.7. Silicon

Silicon has three naturally occurring isotopes being ^{28}Si (92.2%), ^{29}Si (4.7%) and ^{30}Si (3.1%).

Neutron absorption in ^{28}Si and ^{29}Si results in the production of stable isotopes with only ^{30}Si producing the radioactive isotope ^{31}Si which decays to ^{31}P through β^- decay emitting gamma rays at 1 266 MeV as illustrated below.

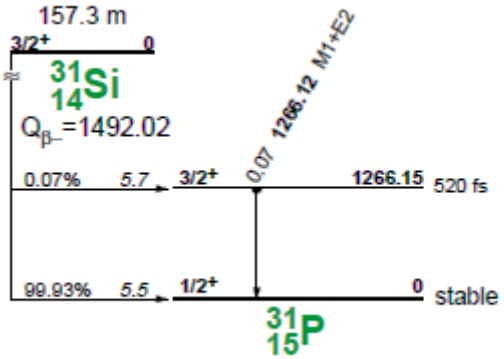

3.3.8. Magnesium

Magnesium has three naturally occurring isotopes being ^{24}Mg (79%), ^{25}Mg (10%) and ^{26}Mg (11%).

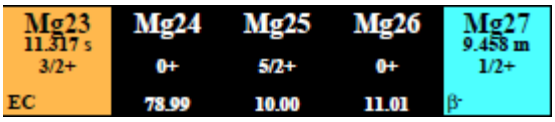

Neutron absorption in ^{24}Mg and ^{25}Mg results in the production of stable isotopes with only ^{26}Mg producing the radioactive isotope ^{27}Mg which decays to ^{27}Al through β^- decay emitting gamma rays at 843.7 and 1014.4 MeV as illustrated below.

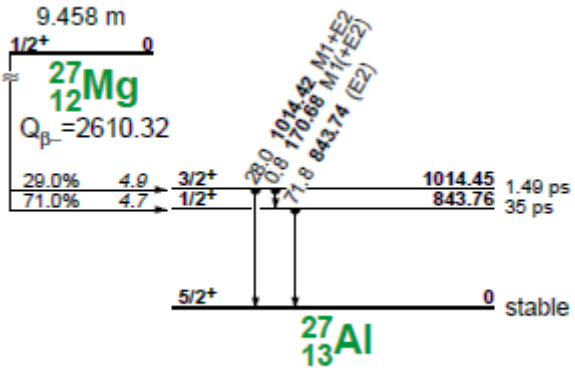

The foregoing assessment of the potential impurities and activation probabilities are summarised combining the composition limits, the stable natural occurring fraction and the thermal neutron absorption cross sections in table 4 below.

Target	Neutron Absorption Cross Section	Parent	Daughter	Decay Mode	Branching	Half life	Gamma Ray Energies				
							Gamma Ray Percentages				
^{50}Ti	0.179	^{51}Ti	^{51}V	β^-		5.76m	320	928.6	608.6		
							93%	6.90%	1.10%		
^{55}Mn	13.36	^{56}Mn	^{56}Fe	β^-		2.578 h	846.8				
							99%				
^{58}Fe	1.32	^{59}Fe	^{59}Co	β^-		44.5 d	1099.3	1291.6			
							53%	45%			
^{63}Cu	4.5	^{64}Cu	^{64}Ni	$e + \beta^+$	61%	12.7h	1345.8				
							100%				
			^{64}Zn	β^-	39%	12.7h	1345.8				
^{65}Cu	2.17	^{66}Cu	^{66}Zn	β^-		5.088m	1039.231	833.5			
							99%	0.22%			
^{64}Zn	0.79	^{65}Zn	^{65}Cu	$e + \beta^+$		244.26d	1115.5				
^{68}Zn	1.07	^{69}Zn	^{69}Ga	β^-		56.4 m	318.7	872.1			
^{70}Zn	0.092	^{71}Zn	^{71}Ga	β^-		2.45 m	511.5	910.2	389.8	121.5	1119.6
							32%	7.80%	3.80%	3%	2.18%
^{30}Si	0.107	^{31}Si	^{31}P	β^-		157.3 m	1226				
							100%				
^{26}Mg	0.0384	^{27}Mg	^{27}Al	β^-		9.458 m	843.7	1014.4			
							72%	28%			
^{50}Cr	15.4	^{51}Cr	^{51}V	e		27.7025 d	320				
							100%				
^{54}Cr	0.41	^{55}Cr	^{55}Mn	β^-		3.497 m	1528.3	2252.4	125.95	1402.4	2239.8
							0.03700%	0.00310%	0.00174%	0.00133%	0.00041%

Table 4 – Summary of target nuclei derived from table 3, naturally occurring stable nuclei, thermal neutron cross sections, decay modes, half-lives and expected gamma ray energies

Chapter 4
Experimental Setup and Methodology

As elaborated on in Chapter 2, the instrumental detection of any particle or radiation depends upon the production of charged secondary particles which can be collected to produce an electrical signal. Charged particles, for example alpha and beta particles, produce a signal within a detector by ionization and excitation of the detector material directly.

Gamma photons are uncharged and consequently cannot directly produce a signal within the detector by ionization and excitation of the detector material. Gamma-ray detection depends upon other types of interaction which transfer the gamma-ray energy to electrons within the detector material. These excited electrons have charge and lose their energy by ionization and excitation of the atoms of the detector medium, giving rise to many electron–hole pairs. The number of electron–hole pairs produced is proportional to the energy of the electrons produced by the primary interaction. The electron–hole pairs are collected by the detector and presented as an electrical signal.

There are several different ways in which gamma-ray photons can interact with matter. In the photoelectric effect, all of the photon energy is transferred to a single electron. In Compton scattering, the photon scatters from an electron transferring some of its energy but re-emerging as a lower-energy photon. In pair production the photon converts to a positron-electron (e^+ e^-) pair.

4.1 Setup and methods

A typical HPGe detector-based gamma spectroscopy system consists of the detector, high voltage power supply, preamplifier, amplifier, Analogue to Digital Converter and multi-Channel Analyser as diagrammatically illustrated in the block diagramme below.

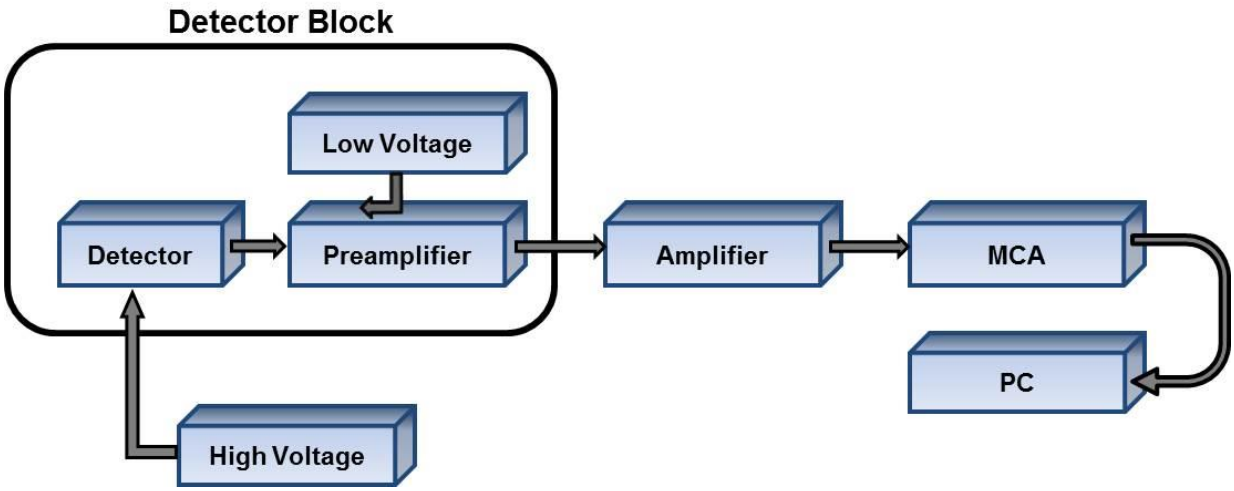

Figure 6 – Block Diagramme of typical Gamma Spectrometry System

As set out in (Reguigui, 2006), the function of the illustrated system and the typical processes are as follows:

- Gamma rays interacts with the detector crystal giving rise to electron–hole pairs;
- The applied bias voltage sweeps the electrons from the crystal;
- The current produced by the electrons creates a pulse signal;
- The preamplifier increases the pulse size;
- The amplifier shapes and further amplifies the pulse;
- The ADC converts the pulse intensity into a numerical value;
- The MCA collects the numerical values per energy category or channel.

4.1.1. Detector

The detector is the centre piece of the gamma spectroscopy system. The Germanium detector is sealed within a vacuum system which is normally manufactured from stainless steel to ensure rigidity and protection of the detector crystal itself. The detector material rests on a thick copper rod commonly referred to as a cold finger as the other end of the copper rod is in thermal contact with liquid nitrogen.

The specific design with the detector housed within a vacuum is to prevent water vapor from the air condensing on the detector with the outside of the container being at room temperature and the detector inside at -196°C. The detector used in the experiment is a high purity germanium gamma ray detector with diameter of 63mm and a length of 63mm housed in a stainless steel casing as indicated in Figure 7.

Figure 7 – Photograph of Germanium Detector used in experiments

4.1.2. Preamplifier

As described in (Reguigui, 2006), the charge that is created within the detector following the gamma ray interaction with the germanium crystal is collected by the preamplifier. The output voltage pulse from the preamplifier is proportional to the input charge received from the detector.

According to (Cherry, Sorenson and Phelps, 2012), the majority of detectors produce relatively small amplitude pulse signals. Based on the physical properties of detectors, they have a high resistance to the flow of electrical currents and signals (i.e. high output impedance). The purpose of a preamplifier is thus threefold:

- to amplify the relatively small detector signal;
- to match the impedance levels between the detector and system components;
- to shape the signal pulse for subsequent signal processing.

4.1.3. High Voltage Supply

From (Reguigui, 2006), the High Voltage Power Supply unit supplies the required high voltage to the detector and the power necessary for the rest of the components to operate.

According to (Reilly, Ensslin and Smith, 1991), the high voltage bias supply provides the electric field that collects the charge generated by the gamma ray interaction in the detector. A typical detector requires a very low current but a high voltage (up to 5 kV). Although the bias supply is not part of the signal path, it is required to operate the detector. The high voltage used during the experiment was set at 4000 V.

4.1.4. Amplifier

From (Reilly, Ensslin and Smith, 1991), the pulses from the gamma rays that leaves the preamplifier are amplified and electronically shaped to meet the requirements of the instrumentation that follows the main amplifier.

The low voltage pulses from the preamplifier are accurately amplified by exactly the same factor into a linear voltage range of typically 0 to 10 V.

To optimise the signal-to-noise ratio, the amplified pulses are electronically shaped to minimise the variation in output pulse amplitude for a given input charge from the preamplifier. Since the multichannel analyser measurement is based on the amplitude of the incoming pulse with reference to an internal reference voltage, the amplifier is designed to quickly return to this stable baseline voltage.

4.1.5. Multichannel Analyser

From (Reguigui, 2006), the multichannel analyser is an indispensable component of experimental measurements as it collects the pulses in all the voltage ranges from the amplifier and stores it as a number corresponding to the various channels. A 4K multichannel analyser will therefore have 4096 channels which can cover an energy region of 0 to 2000 V at a conversion gain of 0.25 keV per channel.

The number of counts per channel is referred to as the pulse height spectrum and forms the basis of the experimental analysis in determining, in this case, the decay energies as the input pulses are sorted by voltage amplitude to form a histogram representing frequency of occurrence versus pulse height.

The Spectrumtechniques UCS30 module which was used in the experiment is shown in Figure 8 in which the ADC and MCA have been combined. The UCS30 is connected via USB cable to a Windows PC which manages the data acquisition and allows some simple analysis.

Figure 8 – Photograph of UCS30 module used during experiment

The oscilloscope is used to measure the shape and size (in volts and time) of the signals coming directly from the PMT.

The oscilloscope is further used to examine quantitatively the relationship between the input(s) and output(s) of each component. The amplifier is adjusted and the effects on the signals produced are observed. The HV and amplifier is adjusted until a reasonable pulse-height spectrum is obtained.

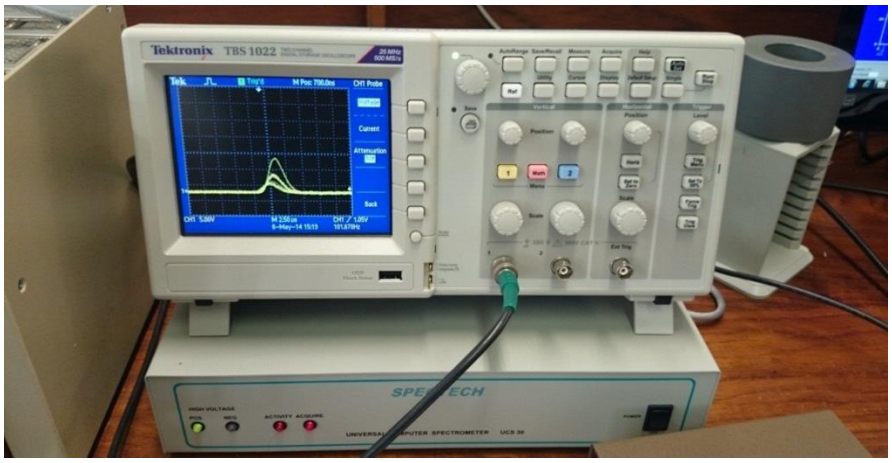

Figure 9 - Photograph of Oscilloscope used during experiment

4.1.6. Calibration Sources

To enable the calibration of the experimental equipment, a set of known gamma-ray sources is used and the main features of the spectrum, in particular the total energy peak, compton edge, and backscatter peak, are noted in terms of channel number and pulse height for calibration of the observed data.

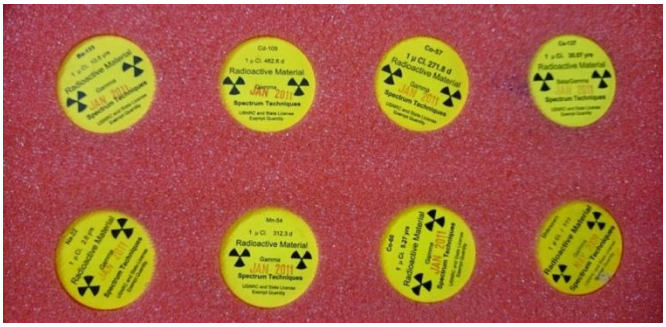

Figure 10 - Known Radiation Sources used for calibration during experiment

The two sources used during the calibration were ^{137}Cs and ^{60}Co. From the TOI (Firestone *et al.*, 1996) it can be seen that ^{137}Cs source beta minus decays to the exited state of ^{137}Ba which in turn de-excites to its ground state through the emission of a gamma ray with energy of 661.66 keV as indicated below.

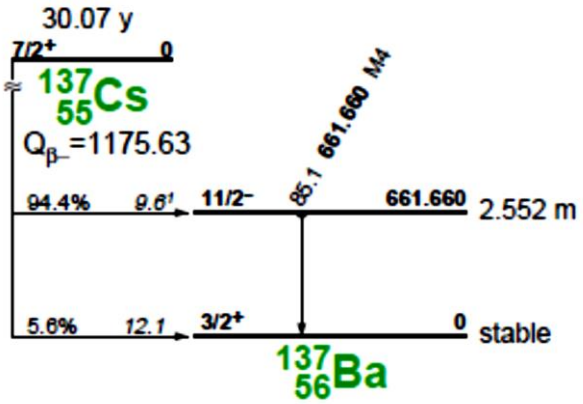

In a similar fashion, the ^{60}Co source beta minus decays to the exited state of ^{60}Ni which de-excites to its ground state through the emission of one or two gamma ray photons with energies of 1173.2 keV and 1332.5 keV as indicated below.

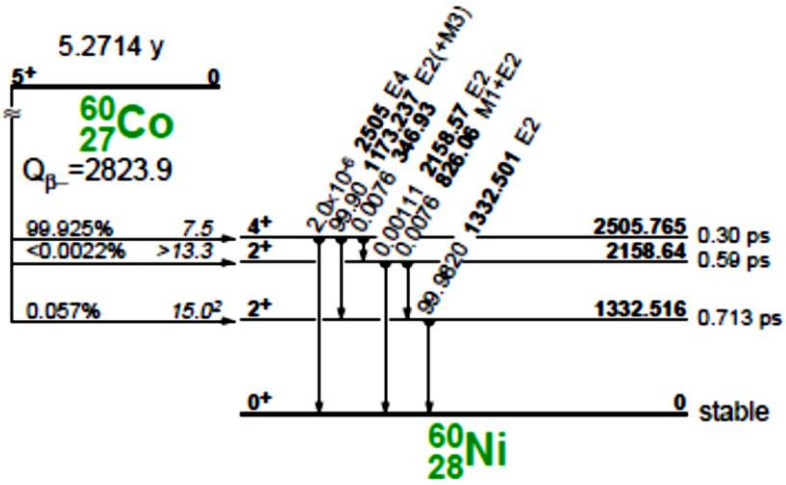

The respective gamma ray energies of 661.66 keV, 1173.2 keV and 1332.5 keV is detected by the Germanium detector and the corresponding channels used for calibration purposes.

4.1.7. AmBe Neutron Source

The specifications and current activity of the AmBe source utilised during the experiment as derived from the PHYLAB_Source_Estimate_Activity data and calculation sheet provided by Dr. Peterson from UCT Physics (private communication), are:

Present Activity	2.04 x 10^{10} Bq
Adjusted Activity Gammas	8.41 x 10^{4} Bq
Adjusted Activity Neutrons	1.53 x 10^{5} Bq
Equivalent Dose	3.33 x 10^{-07} Sv

Radiation can be harmful to living tissue as it can cause damage to biological molecules, particularly DNA (McLean *et al.*, 2017).

To prevent the impact of radiation, the ALARP principle (As Low As Reasonably Practical) should always be applied by reducing radiological exposure by reducing time/duration of exposure, maximizing distance between the source and any living cells, and using appropriate shielding.

Although the AmBe source is a relatively weak source, due care was taken during the conduct of the experiment to limit exposure time and increase distance whenever the source was unshielded by wax or water.

4.1.8. Dipstick Cryostat

Dipstick cryostats consist of a detector chamber having a dipstick-like cold finger which is inserted into a liquid nitrogen Dewar for cooling. The liquid nitrogen loss rate of a typical Dewar is in the region of 0.5 to 0.7 litres/day.

As mentioned in Chapter 2, germanium solid state detectors need to be cooled to liquid nitrogen temperatures to produce accurate and usable spectroscopic data. At higher temperatures, the electrons can easily cross the band gap in the crystal and reach the conduction band, where they are free to respond to the electric field, producing too much electrical noise to be useful as a spectrometer. During the experiment, the detector was cooled to liquid nitrogen temperature (77 K) to reduce thermal excitations of valence electrons so that only a gamma ray interaction can give an electron the energy necessary to cross the band gap and reach the conduction band as depicted in Figure 11 below.

Figure 11 – Filling of the Dewar with liquid nitrogen during the execution of the experiment

4.2 Experiment for Hypothesis 1 – Impurities in the Aluminium

An americium-beryllium (AmBe) radioisotopic source produces neutrons over an energy range from a few eV up to about 11 MeV. The AmBe source is placed in drum of water which is used to moderate (i.e. slow down) the neutrons via multiple elastic collisions with the hydrogen nuclei. A cylinder of natural aluminium is immersed in this neutron bath for about 15 minutes.

Figure 12 – Photograph of the Aluminium cylinder immersed in the neutron bath during the experiment (AmBe source within blue cylinder)

The irradiated aluminium cylinder is removed and placed in front of the germanium detector which produces an electrical pulse which is proportional in height to the energy of the gamma ray deposited in the detector. These electrical signals are amplified, digitised and recorded by a computer.

The initial acquisition mode is set to PHA in which the energy spectrum of the ^{28}Al is recorded, in particular the total energy peak, Compton edge, and backscatter peak are noted in term of channel number and pulse height. Next the acquisition mode is set to multichannel scaling in which all the pulses entering the counting system are summed for a fixed time interval on a continuous basis which will be used to derive the decay coefficient and half-life of the different elements as part of the Neutron Activation Analysis.

The radiation safety requirements to ensure that the exposure is kept as low as reasonably achievable was ensured by minimising the handling of the AmBe source, by increasing the distance to the source through handling the source by the attached ropes and by evacuating the area whilst the source was in the neutron bath. The area was also secured to ensure that no unauthorised access was gained to the AmBe source.

The experiment was performed in the Nuclear Physics laboratories in the Physics Department at the University of Cape Town. The experiment was first attempted in March 2016 but was not concluded due to challenges with the supply of liquid Nitrogen. Two further attempts were performed on 5 April 2016 and 9 June 2016. Challenges experienced with the MCS mode of the Multi-Chanel Analyser rendered inconsistent data not suitable for analysis. A fourth attempt was made on 28 June 2016. The MCS mode challenges persisted. The experimental data required was obtained by manually saving the recorded data at 30 second intervals. The data was normalised from the actual dwell times to the intended 30 second dwell time.

4.3 Experiment for Hypothesis 2 – Inadequate Moderation

As the experiment involves the use of an unmoderated neutron source, the area for the experiment is made safe to prevent the inadvertent radiation of any persons and to prevent the unauthorised access and potential loss of source.

The AmBe source is placed within the aluminium cylinder on a table. With no water to moderate the neutrons produced by the source and only an air gap between the source and the target, the aluminium is irradiated with fast neutrons.

The irradiated aluminium is placed close to the germanium detector and the acquisition mode is set to multichannel scaling in which all the pulses entering the counting system are summed for fixed time intervals on a continuous basis for subsequent analysis.

The experiment was conducted in the Nuclear Physics laboratories in the Physics Department at the University of Cape Town on the same dates and safety precautions as stated for hypothesis 1.

Chapter 5
Experimental Results

5.1 Hypothesis 1 – Impurities in the Aluminium

5.1.1 Energy Calibration

For all energy measurements, it is necessary to have an energy scale to which the counting bins are referenced. In gamma-ray spectrometry with HPGe detector running on PCA3, the pulse height scale is present in a channel number. In order to convert channel position to energy scale, the energy calibration was carried out by using standard radioactive calibration sources which produce gamma rays at well-known and precisely measured energies as stated in 4.1.6. The energy spectra of the two sources used, being Cobalt and Cesium, are shown in Figures 13 and 14.

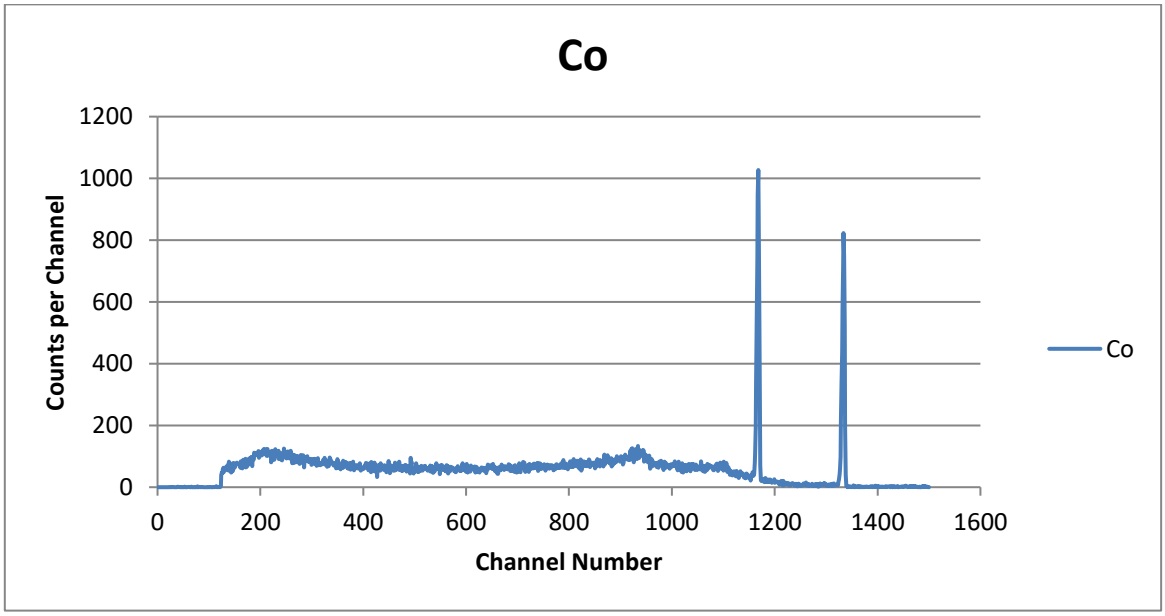

Figure 13 – Plot of the count rate from the Cobalt calibration source

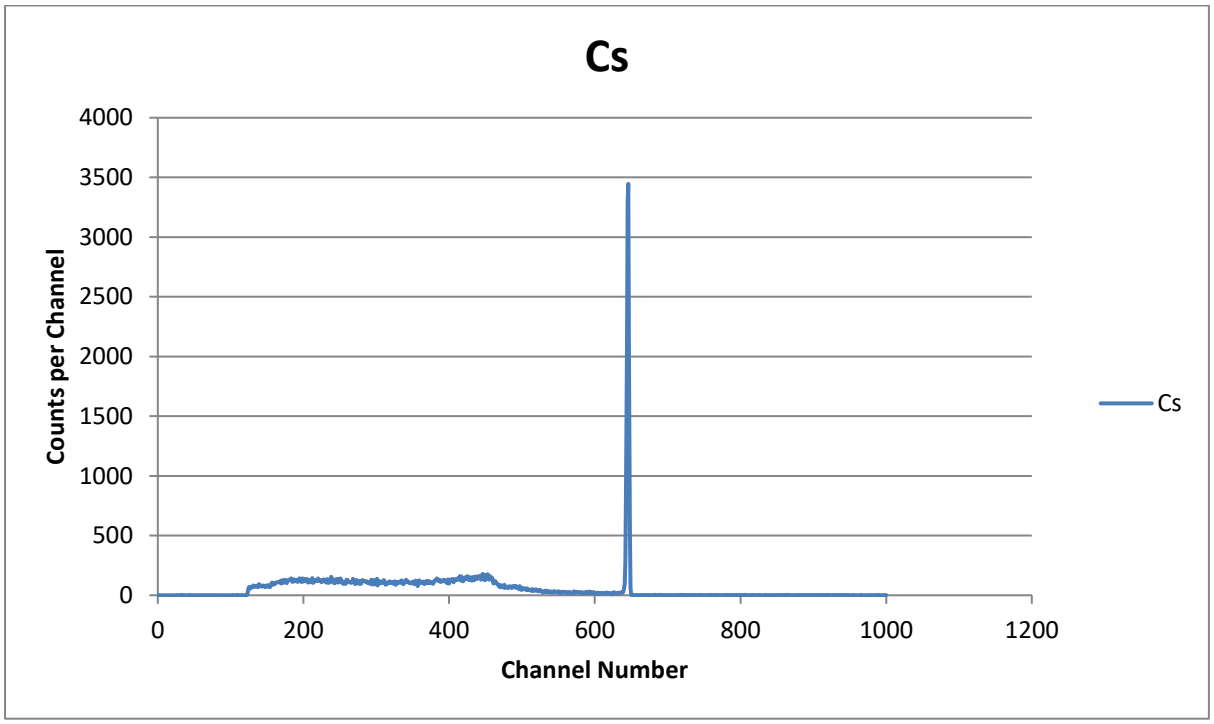

Figure 14 – Plot of the Cesium calibration source

The peak from the ^{137}Cs source is observed at channel 646 and the two peaks for ^{60}Co source at channels 1168 and 1334. The observed peaks correspond with the expected decay energies of 661.7, 1173.2 and 1332.5 keV respectively as indicated in Table 5 and plotted in Figure 15.

Source	Peak	Expected E (keV)
^{137}Cs	646	661.7
^{60}Co	1168	1173.2
^{60}Co	1334	1332.5

Table 5 – Calibration relation between peak channel and expected decay energy

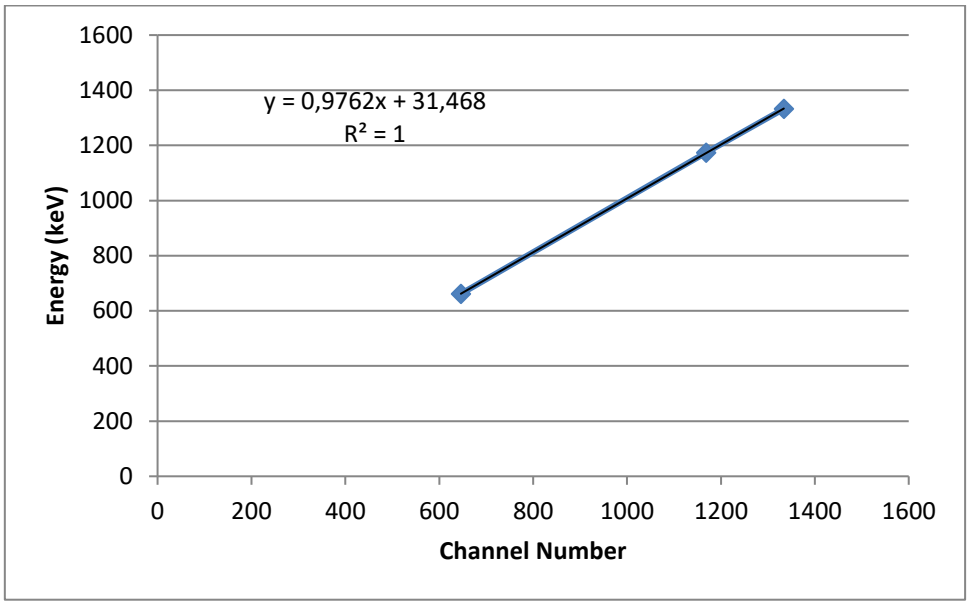

Figure 15 – Calibration plot of channel number against expected decay energy

From Figure 15, the relationship between the decay energy and channel number is derived as the linear function:

$$Y = 31.468 + 0.9762 * X \quad (5.1)$$

where Y is the energy corresponding to channel number X.

The relevant energies were calculated from the channel / energy relationship and utilised instead of the channel numbers.

5.1.2 Spectrum Analysis and Nuclides Identification

After the energy calibration was completed, a decay spectrum was obtained from the data recorded. Although the anticipated 1778 keV gamma ray is expected to decrease with a 138 second half-life, the count was run for a full 30 minutes. The overall gamma ray spectrum is illustrated in the Figure 16.

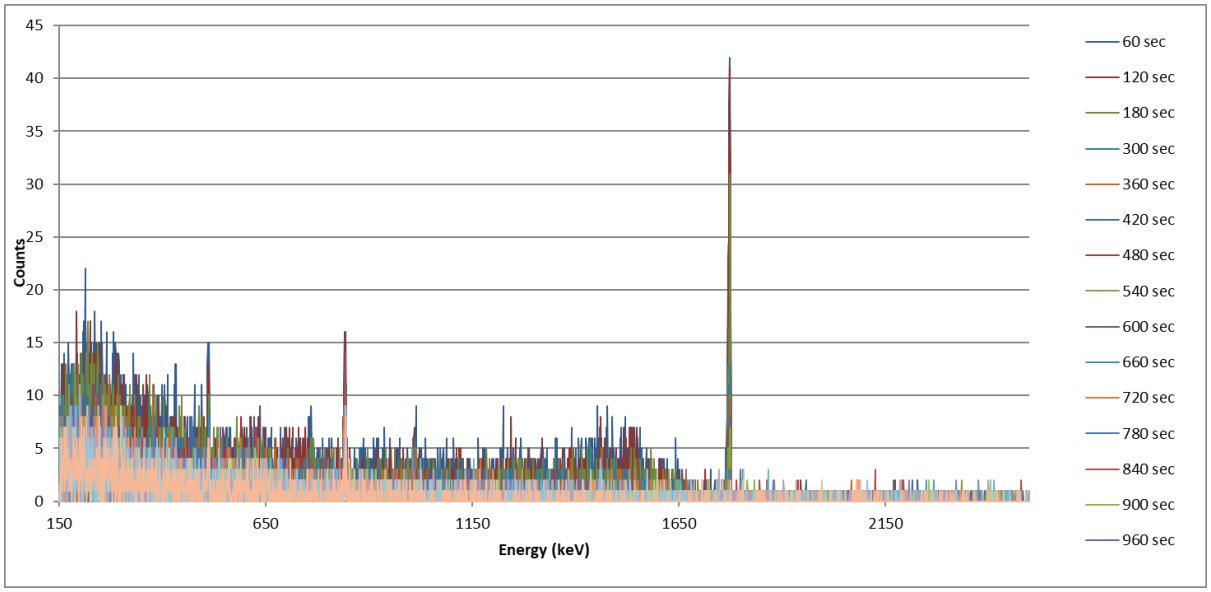

Figure 16 – Gamma ray spectrum from thermal neutron activated aluminium cylinder

The spectrum was analysed and a number of significant peaks identified for further analysis as represented in Figures 17 - 20 below.

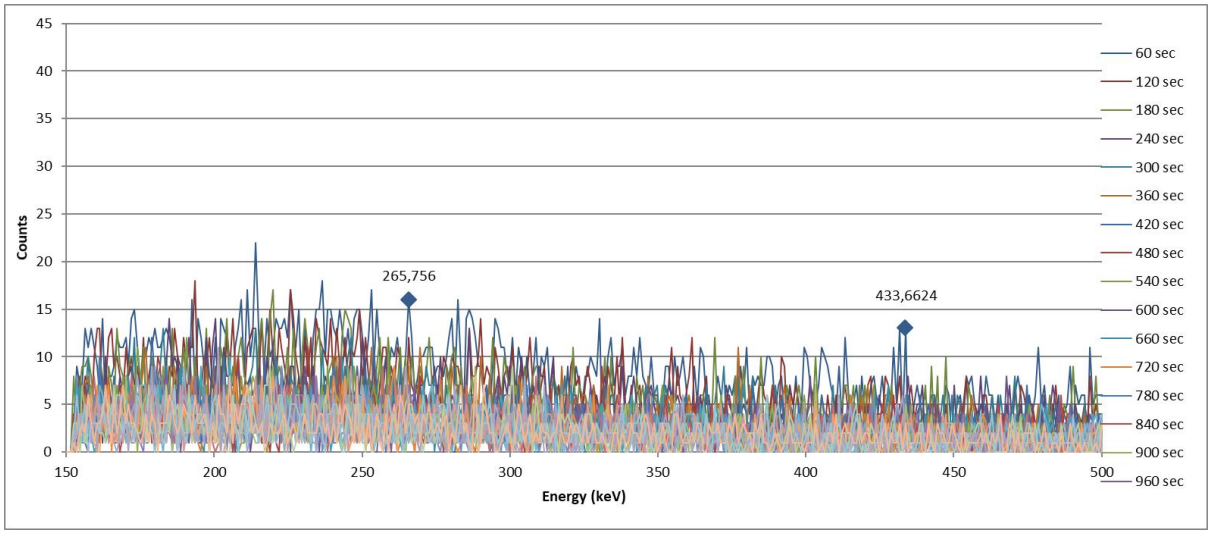

Figure 17 - Gamma ray spectrum up to 500 keV from activated aluminium cylinder

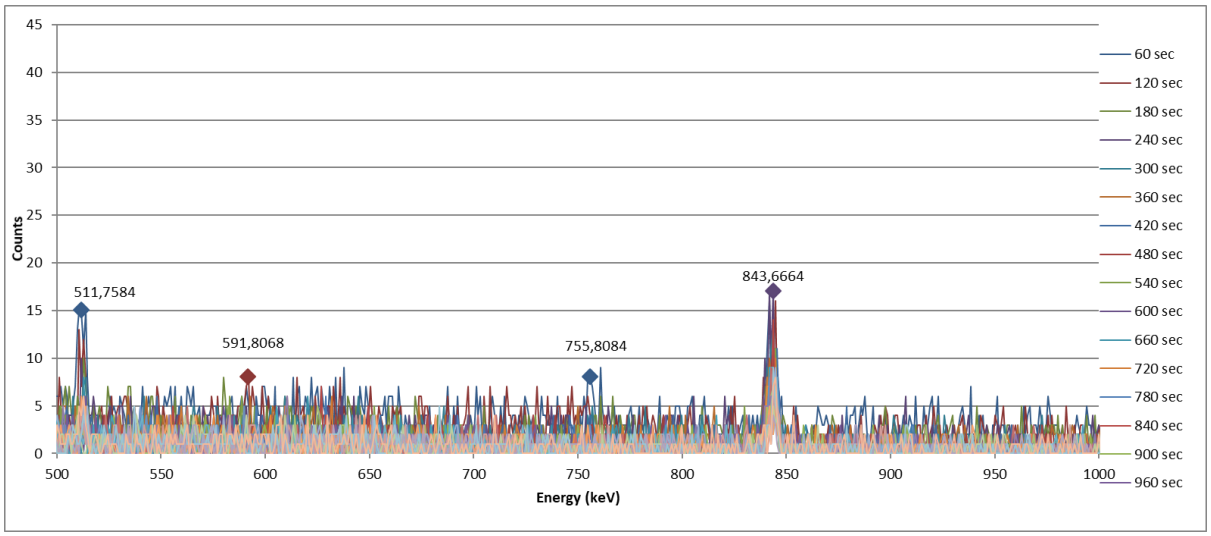

Figure 18- Gamma ray spectrum from 500-1000 keV from activated aluminium cylinder

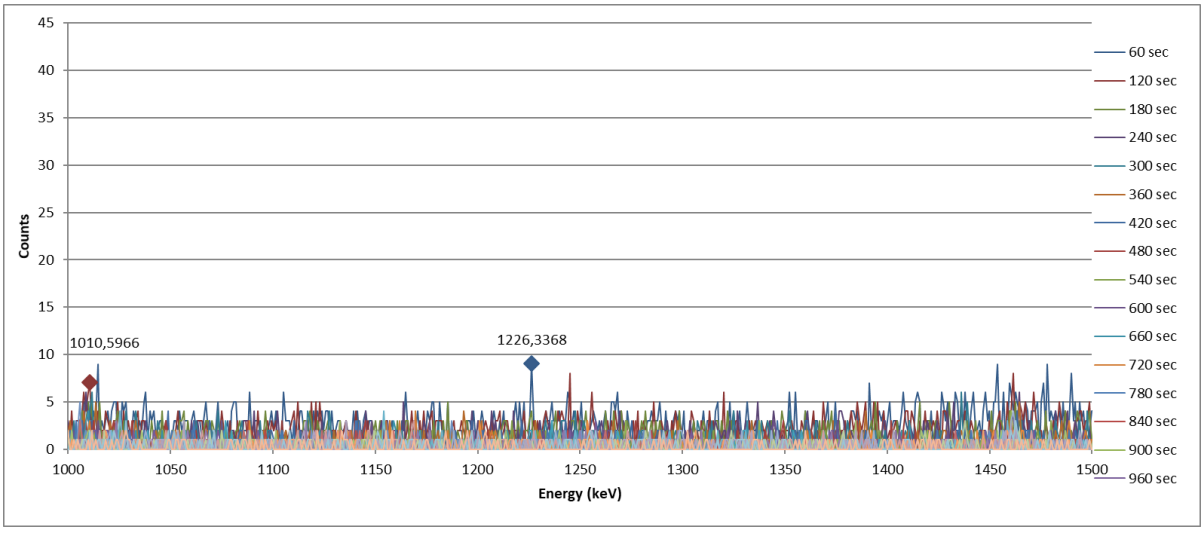

Figure 19- Gamma ray spectrum from 1000-1500 keV from activated aluminium cylinder

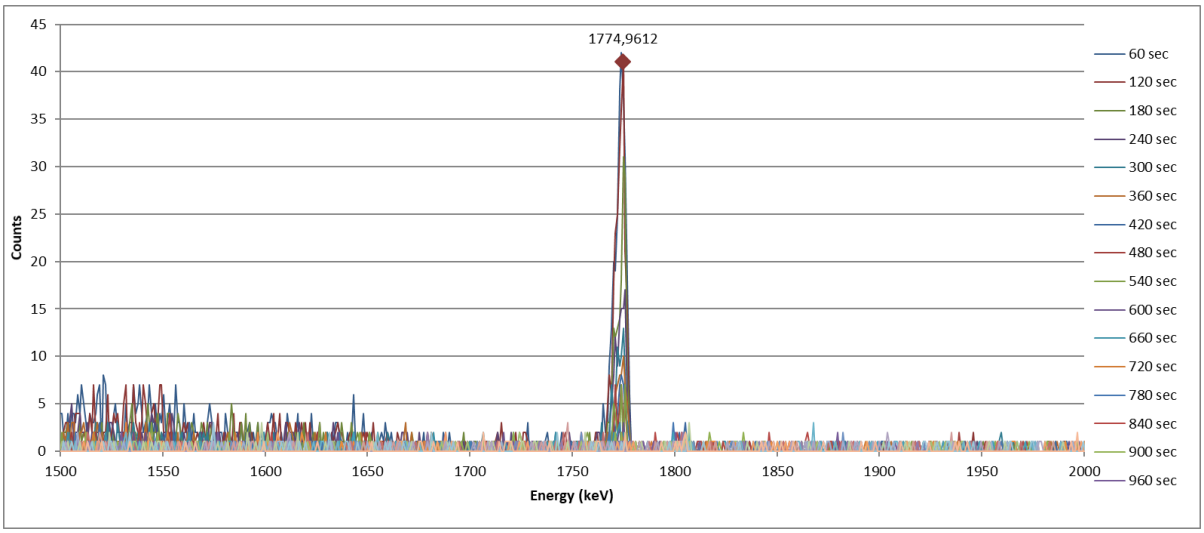

Figure 20 - Gamma ray spectrum from 1500-2000 keV from activated aluminium cylinder

The following significant peaks were identified from the gamma ray spectrum:

265.7 keV
433.7 keV
511.8 keV
591.8 keV
755.8 keV
843.7 keV
1010.6 keV
1226.3 keV
1775 keV

These energies were compared to the anticipated gamma rays from the typical impurities and alloying materials as summarised in Table 4. As the hypothesis is only trying to demonstrate the measurement of gamma rays emanating from the decay from the activation of material other than Aluminium, a full spectrum analysis is not attempted. The following potential impurities were selected and are further analysed for comparison with the measured and anticipated half-lives.

Measured Energy (keV)	Parent	Daughter	Gamma Ray Energy (keV)
511.8	^{71}Zn	^{71}Ga	511.5
843.7	^{27}Mg	^{27}Al	843.7
	^{56}Mn	^{56}Fe	846.8
1010.6	^{27}Mg	^{27}Al	1014.4
1226.3	^{31}Si	^{31}P	1226
1775	^{28}Al	^{28}Si	1780

Table 6 – Measured vs anticipated gamma ray energies

5.1.3 Half-Life

Plotting the results of the observed counts at 1775 keV against time yields the relationship depicted below.

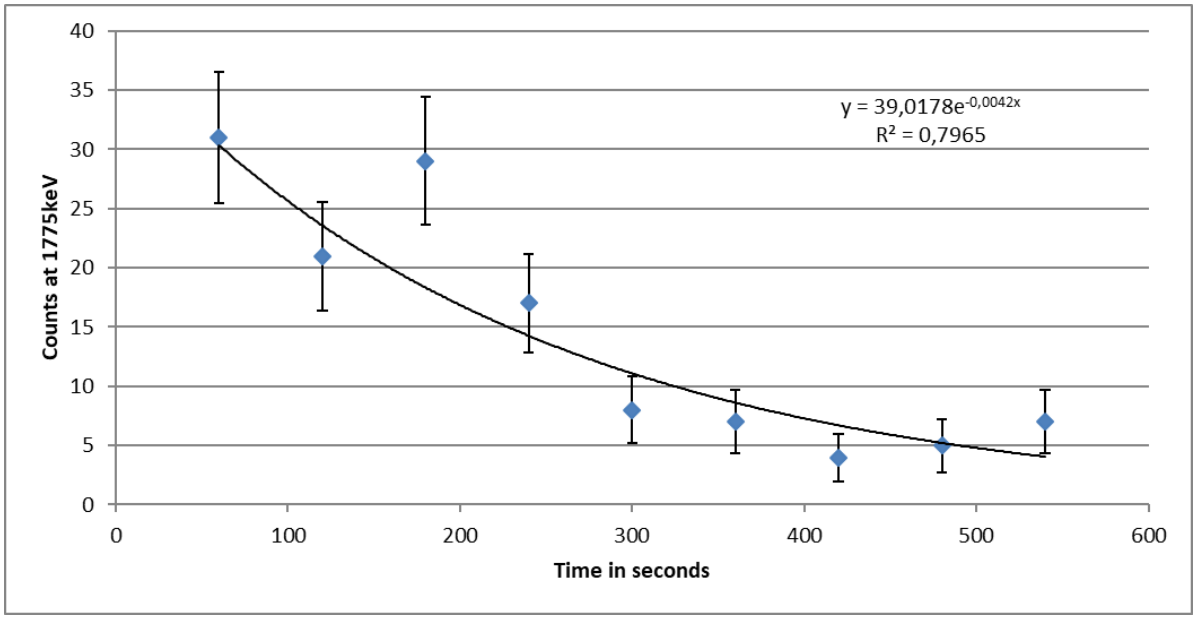

Figure 21 – Plot of observed counts at gamma energy of 1775 keV against time

The best fit through the plot yields the following exponential relationship:

$$y = 39.0178e^{-0.0042x} \quad (5.2)$$

Plotting the natural logarithm of the various observed decays against time (i.e. a semi logarithmic plot) yields a linear relationship as shown below for the 1775 keV decay readings.

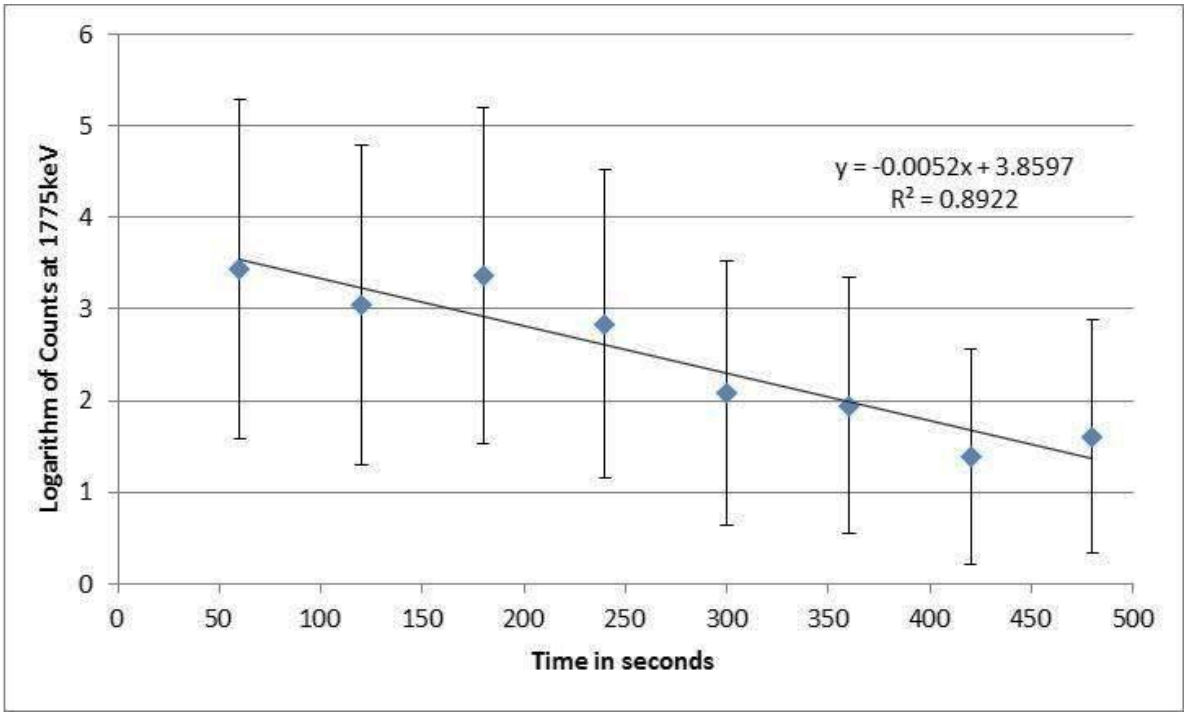

Figure 22 – Plot of natural logarithm of observed counts at Gamma energy of 1775 keV

In a similar fashion, the decay relationships for the various observed energies of interest were determined and are tabulated below.

Energy	Relationship based on exponential fit Relationship based on linear fit to the natural logarithm	R-squared value
511keV	$y = 12.0544e^{-0.0049x}$	$R^2 = 0.2838$
	$y = -0.0049x + 2.4894$	$R^2 = 0.2838$
843keV	$y = 10.3781e^{-0.0013x}$	$R^2 = 0.3126$
	$y = -0.0013x + 2.3397$	$R^2 = 0.3126$
1010keV	$y = 10.0178e^{-0.0056x}$	$R^2 = 0.8483$
	$y = -0.0056x + 2.3191$	$R^2 = 0.8961$
1226keV	$y = 8.2018e^{-0.0062x}$	$R^2 = 0.4944$
	$y = -0.0062x + 2.1044$	$R^2 = 0.4944$
1775keV	$y = 39.0178e^{-0.0042x}$	$R^2 = 0.7965$
	$y = -0.0052x + 3.8597$	$R^2 = 0.8922$

Table 7 – Decay Relationships per energy of interest

Although the exponential and logarithmic functions are inverse functions of each other, the determination of the decay constant from the plot of the natural logarithm of the various observed decays against time is not 100% accurate as the fitting algorithms assume a natural distribution of the uncertainties. The uncertainty is however deemed very small and the calculated decay constant is considered as acceptable for all practical purposes.

The half-life of an isotope was described in Chapter 2 and defined as:

$$t_{½} = \ln(2) / \lambda \qquad (5.3)$$

The best fit through the semi logarithmic plot of the observed count rate yields the following linear relationship:

$$y = -0.0052x + 3.8597 \qquad (5.4)$$

The slope of the trend line is -0.0052 and represents the decay constant (the negative representing a decaying relationship).

Substituting $\lambda = 0.0052$ into equation (5.3)

$t_{½} = \ln(2) / \lambda$

$= \ln(2) / 0.0052$

$= 133.3$ sec

From the different decay relationships in Table 7 and equation 5.2, the following decay constants and half-lives are calculated:

Energy	Decay Constant (s^{-1})	Half Life (s)
511 keV	0.0049	141.5
843 keV	0.0013	533.2
1010 keV	0.0056	123.8
1226 keV	0.0062	111.8
1775 keV	0.0052	133.3

Table 8 – Decay Constants and Half Lives per energy of interest

The expected decay energies and half-lives for the isotopes of interest are tabulated against the calculated half-lives and measured decay energies below:

Parent	Daughter	Expected Gamma Ray Energy (keV)	Measured Decay Energy (keV)	Published Half-Life (seconds)	Half-Life based on Gradient of Logarithmic plot (seconds)
^{71}Zn	^{71}Ga	511.5	511.7	147.0	141.5
^{27}Mg	^{27}Al	843.7	842.7	567.5	533.2
^{27}Mg	^{27}Al	1014.4	1009.6	567.5	123.8
^{31}Si	^{31}P	1226	1226.3	9438.0	111.8
^{28}Al	^{28}Si	1780	1775.9	134.5	133.3

Table 9 – Tabulated comparison of expected decay energies and published half-lives with measured decay energies and half-lives derived from gradient of logarithmic plot

5.2 Hypothesis 2 – Inadequate Moderation

The same calibration as for hypothesis 1 experiment was performed to establish an energy scale to which the counting bins are referenced.

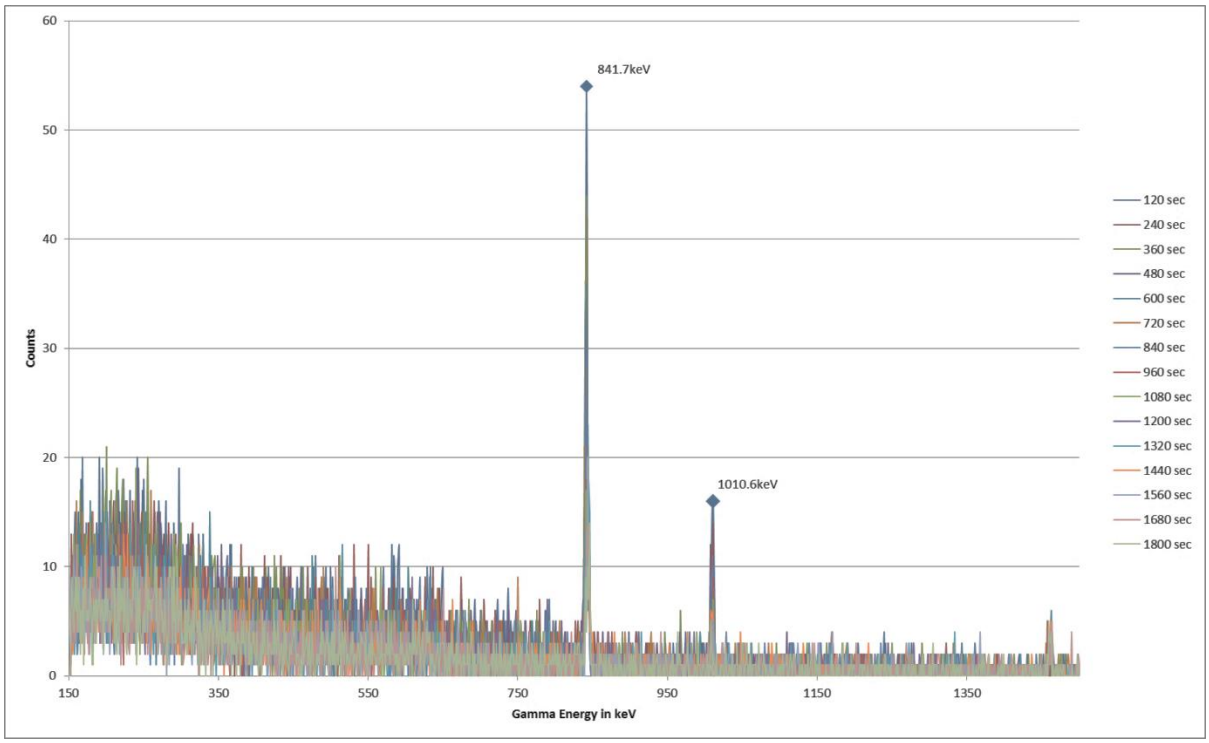

Figure 23 – Gamma ray spectrum from fast neutron activated aluminium cylinder

The two gamma ray energies associated with the decay of ^{27}Mg being 843.7 and 1014.4 keV are indicated and further interrogated.

From the moderated neutron source, the following counts are observed for the two energies of interest:

841 keV – 185 counts in 1803 seconds

1010 keV – 47 counts in 1803 seconds

From the unmoderated neutron source, the following counts are observed for the two energies of interest:

841 keV – 345 counts in 1804 seconds

1010 keV – 104 counts in 1804 seconds

The unmoderated neutron source resulted in a significantly higher count rate (86.4% and 121.3%) when compared to the count rate observed from the decay from activation by the moderated neutron source.

Chapter 6
Discussion of Results

The decay spectra that were obtained from the data recorded for the two hypotheses tested are typical gamma ray spectra as reflected in figures 16 and 23 in Chapter 5.

As described in (Gilmore, 2008), all the significant interaction processes (i.e. photoelectric absorption, compton scattering and pair production) result in the transfer of gamma ray energy to electrons in the absorbing medium which in this case is the germanium detector. The energy transferred to the electrons represents the energy absorbed in the detector (assuming no leaked energy out the sides or back of the detector which is not an unreasonable assumption as the experiment made use of a fairly large detector with a diameter of 63mm and a length of 63mm) and thus the output from the detector. Photoelectric interactions are dominant at low energy and pair production at high energy, with Compton scattering being most important in the mid-energy range.

In photoelectric absorption, the incoming gamma-ray transfers virtually all of its energy to an atomic electron (usually the most tightly bound electron) of an atom which is ejected from the atom. The energy of the ejected electron is equal to the energy of the initial gamma-ray minus the binding energy for the atomic electron. The ejected electron is detected as a full energy peak in the energy spectrum which facilitates the measurement of the energy of a gamma-ray photon.

In Compton scattering the incoming gamma ray interacts with an atomic electron and transfers a fraction of its energy to the electron. The gamma ray is deflected through an angle ranging from 0° to 180° from its original path whilst he scattered gamma ray continues with the remaining energy. The electron that absorbed the energy from the gamma ray is ejected from the atom. The energy transferred to the electron is

dependent on the scattering angle and can be detected as the Compton continuum in the energy spectrum.

Pair production is a result of the interaction of the gamma ray with the atom as a whole, resulting in the conversion of a gamma-ray into an electron–positron pair. Pair production is only possible if the incident gamma ray photon has an energy that exceeds twice the combined rest mass energy of the electron and positron pair (i.e. 1022 keV). This energy can be observed as the pair production peak in the energy spectrum.

6.1 Hypothesis 1

From (Gilmore, 2008), gamma-rays are emitted with very precisely defined energies which is characteristic of a particular radionuclide. As discrimination between radionuclides by gamma energy alone could be a challenge where isobaric nuclides are decaying to the same stable product from either side, a further nuclear parameter which can be utilised to distinguish between the decay of different nuclides is the half-life.

From table 9, a strong correlation between the published decay energies for certain of the alloying elements typically found in aluminium and the measured energy peaks is observed. This correlation would indicate that certain of the measured additional energies observed during the experiment could be from the decay of materials other than the intended ^{28}Al.

Parent	Daughter	Expected Gamma Ray Energy (keV)	Measured Decay Energy (keV)
^{71}Zn	^{71}Ga	511.5	511.7
^{27}Mg	^{27}Al	843.7	842.7
^{56}Mn	^{56}Fe	846.8	842.7
^{27}Mg	^{27}Al	1014.4	1009.6
^{31}Si	^{31}P	1226	1226.3
^{28}Al	^{28}Si	1780	1775.9

Table 10 – Tabulated comparison of expected and measured decay energies

The 511 keV gamma is most probably due to processes which lead to the production of positrons such as beta plus decay and pair production which are briefly described below.

Positrons, which are the antiparticle counterpart to electrons, are regularly created during nuclear beta plus decay. In beta plus decay a proton inside a nucleus with too many protons is converted into a neutron while releasing a positron and an electron neutrino. This reduction in the amount of protons will move the product closer to the region of stability.

Positron emission typically occurs in large "proton-rich" radionuclides which decreases the proton number relative to neutron number. Positron emission therefor results in a nuclear transmutation in which an atom of one chemical element is transmutated into an atom of an element with an atomic number that is less by one unit as indicated diagrammatically below:

$$^{22}\mathrm{Na} \rightarrow {}^{22}\mathrm{Ne} + \mathrm{e}^{+} + \bar{\nu}_{\mathrm{e}}$$

Positrons can also be created by high energy gamma rays in a process known as pair production. Pair production occurs when a sufficiently energetic gamma ray interacts with a nucleus and converts the energy of the gamma ray into mass according to Einstein's special-relativity equation $E = mc^2$. The incident gamma ray

must have sufficient energy of at least the combined rest masses of the two created particles. For pair production to occur the total energy of the incident gamma ray must therefore be at least 1.022 MeV.

When a positron is surrounded in matter it has a short lifetime since it will quickly lose energy by ionization, slow down, attract an electron and annihilate. When a positron and an electron interact, they may form Positronium which is stable for nanoseconds before annihilating, or else the pair annihilate directly. During the annihilation, all of the mass energy of the positron and the electron is converted into gamma ray energy according to Einstein's special-relativity equation $E = mc^2$. Based on the rest mass of the two particles being annihilated, this will typically result in two 511 keV gamma rays which travel away, back to back, from the annihilation point.

Evaluating the other nuclear parameter which can be utilised to distinguish between the decay of different nuclides, i.e. the half-life, a very weak correlation is observed between the published half-lives for the alloying elements and the half-lives derived from the gradients of the semi logarithmic plot of the various measured decays against time as indicated in the table below:

Parent	Daughter	Published Half-Life (seconds)	Half-Life based on Gradient of Logarithmic plot (seconds)
^{71}Zn	^{71}Ga	147.0	141.5
^{27}Mg	^{27}Al	567.5	533.2
^{56}Mn	^{56}Fe	9280.8	
^{27}Mg	^{27}Al	567.5	123.8
^{31}Si	^{31}P	9438.0	111.8
^{28}Al	^{28}Si	134.5	133.3

Table 11 – Tabulated comparison of published half-lives with half-lives derived from gradient of logarithmic plot

Only the decay half-lives of ^{71}Zn, ^{27}Mg and ^{28}Al show comparable results.

6.2 Hypothesis 2

^{27}Mg can be formed through either the absorption of thermal neutrons by the isotope ^{26}Mg or through the ^{27}Al (n,p) ^{27}Mg reaction where a proton is produced promptly after neutron capture leaving ^{27}Mg.

To produce ^{27}Mg with thermal neutrons, the ^{26}Mg isotope has to capture a neutron. With only 11% of naturally occurring Mg being the isotope ^{26}Mg and thermal absorption cross section being a low 0.0384 barn coupled with a relatively low presence as an impurity in Aluminium (maximum range being 0.5 – 5.1%), although possible - this is the less probable process to be producing ^{27}Mg.

The production of ^{27}Mg with fast neutrons through the ^{27}Al (n,p) ^{27}Mg reaction is much more probable as the target nuclei abundance is 170 times higher for ^{27}Al than ^{26}Mg and the cross section for the reaction increases drastically as the incident neutron energy increases as indicated in the figure below.

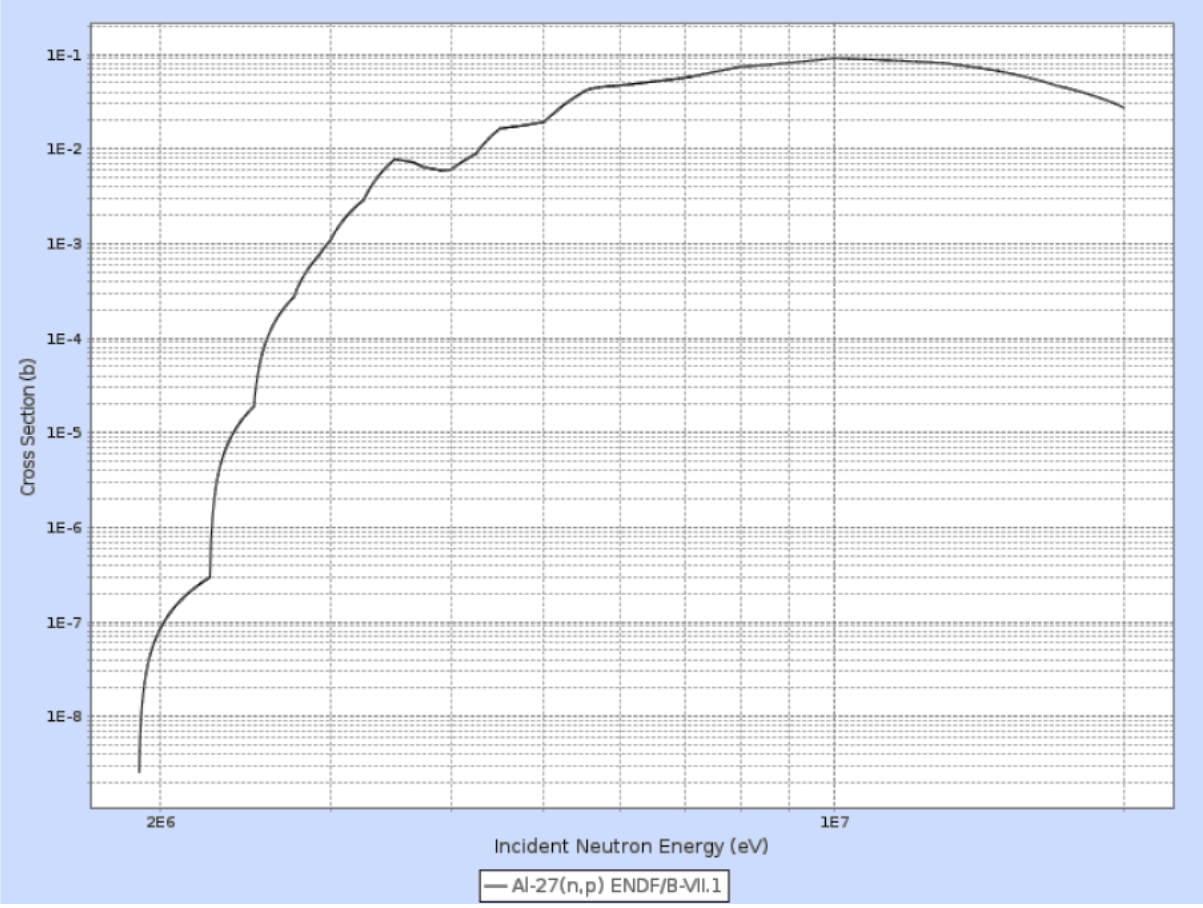

Figure 23 – ^{27}Al (n,p) ^{27}Mg cross section vs Incident Neutron Energy (Atom.Kaeri)

As noted in the results in section 8.2, the unmoderated neutron source resulted in a significantly higher count rate (86.4% and 121.3% higher) when compared to the count rate observed from the decay from activation by the moderated neutron source.

The count rate is directly proportional to the strength of the radioactive source, the latter which is defined as the number of disintegrations per second (one becquerel (Bq) being defined as one disintegration per second).

The significant increase in the activity of the activated Aluminium associated with ^{27}Mg resulting from the unmoderated neutron source is a clear indication that the decay energies observed in the decay following activation from the moderated neutron source.

Simply put – seeing the same but increased decay energy peaks in the unmoderated experiment as in the moderated experiment means there are unmoderated neutrons in the moderated experiment.

Chapter 7
Conclusions

Based on the results of the two experiments conducted as described in this mini-dissertation, it has been demonstrated that there is some evidence, though not very convincing, that both postulated hypotheses are potentially possible.

Considering the relatively small amounts of alloying elements in a typical aluminium sample and the poor correlation between published half-lives with the derived half-lives from the experiment as discussed in section 6.1, the hypothesis that the impurities in the aluminium from which the aluminium cylinder is manufactured are activated when immersed in the neutron bath resulting in the measurement of the decay of materials other than the intended ^{28}Al, is considered possible but improbable.

On the other hand, considering the pertinence of the decay signature of ^{27}Mg in both experiment, the observed increase in the ^{27}Mg activity in the unmoderated activation, the abundance of the target nuclei of ^{27}Al, as well as the increase in the ^{27}Al (n,p) ^{27}Mg reaction with increased neutron energy as discussed in section 6.2, hypotheses 2 is deemed both possible and probable.

Based on the results obtained and discussed, it is therefore concluded that the additional energy readings observed during the execution of the nuclear physics experiment to determine the half-life of activated ^{28}Al is contributable to the incomplete moderation of the neutrons during the experiment and hence the formation and subsequent decay of ^{27}Mg instead of the intended ^{28}Al.

Further work can be conducted to improve the deductions derived in this dissertation by amongst others, increasing the number of trials to obtain different data sets which

can be statistically analysed to help address the probabilistic nature of radioactive decay, increasing the number of runs to provide more data for the time spectra to be able to calculate the lifetimes to usable precision, reducing systematic errors from background radiation through adequate shielding, increasing the amount of gamma rays in the activation spectrum through increased activation levels of the trace elements by utilising stronger neutron sources and by improving the analytical techniques through the use of superior software.

References

AluMatter (2013) *aluMATTER | Aluminium | Property Definitions | Hardness*. Available at: https://archive.is/Zbgvg (Accessed: 21 March 2018).

Bodansky, D. (2004) *Nuclear Energy*. Springer New York. doi: http://sci-hub.tw/10.1007/b138326.

Cherry, S., Sorenson, J. and Phelps, M. (2012) *Physics in Nuclear Medicine*, *Physics in Nuclear Medicine*. Elsevier. doi: 10.1016/C2009-0-51635-2.

Davis, J. R. (2001) 'Aluminum and Aluminum Alloys', *Light Metals and alloys*, p. 66. doi: 10.1361/autb2001p351.

Dawson, D., Fleck, A. and Wadham, A. (1993) *Radiation Damage to Materials*, *Course 228*. Available at: https://canteach.candu.org/Content Library/20040904.pdf (Accessed: 10 March 2018).

Eby, N. (2017) *Instrumental Neutron Activation Analysis (INAA)*. Available at: https://serc.carleton.edu/research_education/geochemsheets/techniques/INAA.html (Accessed: 10 March 2018).

Firestone, R. B. *et al.* (1996) *Table of Isotopes (A=263-272) † CD ROM Edition*. Available at: https://www.wiley.com/legacy/products/subject/physics/toi/toi.pdf (Accessed: 7 January 2019).

Gilmore, G. R. (2008) *Practical Gamma-Ray Spectrometry*, *Practical Gamma-Ray Spectrometry*. Wiley. doi: 10.1002/9780470861981.

Global Metals (2011) *Precision metal fabrication*. Available at: http://www.globalmetals.com/index.html (Accessed: 10 March 2018).

Hamidatou, L. *et al.* (2013) 'Concepts, Instrumentation and Techniques of Neutron Activation Analysis', in *Imaging and Radioanalytical Techniques in Interdisciplinary Research - Fundamentals and Cutting Edge Applications*. InTech, pp. 75–100. doi: 10.5772/53686.

IAEA-TECDOC-1340 (2003) *Manual for reactor produced radioisotopes*. IAEA. Available at: http://www.isotopes.gov/outreach/reports/Reactor_Isotopes.pdf (Accessed: 10 March 2018).

Keisach, B. (1972) *The Atomic Fingerprint: Neutron Activation Analysis*. Available at: https://www.gutenberg.org/files/48406/48406-h/48406-h.htm (Accessed: 10 March 2018).

Lewis, E. E. (2008) *Fundamentals of Nuclear Reactor Physics*, *Fundamentals of Nuclear Reactor Physics*. doi: 10.1016/B978-0-12-370631-7.X0001-0.

Lilley, J. S. (John S. . (2001) *Nuclear physics : principles and applications*. J. Wiley. Available at: https://www.wiley.com/en-za/Nuclear+Physics:+Principles+and+Applications-p-9780471979364 (Accessed: 18 July 2018).

Live chart - Table of Nuclides - Nuclear structure and decay data (2018) *IAEA*. Available at: https://www-nds.iaea.org/relnsd/vcharthtml/VChartHTML.html (Accessed: 8 January 2019).

Marsh, J. W., Thomas, D. J. and Burke, M. (1995) *High resolution measurements of neutron energy spectra from Am-Be and Am-B neutron sources*. Available at: https://zzz.physics.umn.edu/lowrad/_media/ambe_marsh_nima_1995.pdf (Accessed: 7 January 2019).

Martin, B. R. (2006) *Nuclear and Particle Physics*, *Nuclear and Particle Physics*. doi: 10.1002/0470035471.

McLean, A. R. *et al.* (2017) 'A restatement of the natural science evidence base concerning the health effects of low-level ionizing radiation', *Proceedings of the Royal Society B: Biological Sciences*, 284(1862), p. 20171070. doi: 10.1098/rspb.2017.1070.

Murray, R. L. and Holbert, K. E. (2015) ‘Chapter 3 - Radioactivity’, *Nuclear Energy (Seventh Edition)*, pp. 31–46. doi: http://dx.doi.org/10.1016/B978-0-12-416654-7.00003-4.

Nuclear Physics - Department of Physics - University of Liverpool (no date). Available at: https://www.liverpool.ac.uk/physics/research/nuclear-physics/ (Accessed: 22 October 2018).

Odeblad, E. and Nati, G. (1955) ‘Detection of Beryllium by Means of the Be9 (α, nγ)C12 Reaction, Acta Radiologica’. doi: 10.3109/00016925509172768.

Reguigui, N. (2006) *Gamma Ray Spectroscopy - Practical Information*. Available at: https://www.scribd.com/document/69061179/Gamma-Ray-Spectroscopy (Accessed: 10 June 2018).

Reilly, D., Ensslin, N. and Smith, H. (1991) *Passive Nondestructive Assay of Nuclear Materials*. Edited by S. Kreiner.

The Aluminum Association (2018) *The Aluminum Association*. Available at: http://www.aluminum.org/ (Accessed: 11 August 2018).

TRIUMF (no date) *Radioactive Decay Modes*. Available at: http://www.triumf.ca/radioactive-decay-modes (Accessed: 18 July 2018).

United Aluminium (2013) *Chemical Composition and Properties of Aluminum Alloys - United Aluminum*. Available at: https://www.unitedaluminum.com/chemical-composition-and-properties-of-aluminum-alloys/ (Accessed: 10 March 2018).

USNRC (2009) *Neutron Activation and Activation Analysis*. Available at: https://www.nrc.gov/docs/ML1122/ML11229A714.pdf (Accessed: 21 March 2018).